

Review

The Use of Magnetic Porous Carbon Nanocomposites for the Elimination of Organic Pollutants from Wastewater

Bendi Anjaneyulu ¹, **Ravi Rana** ², **Versha** ^{2,*}, **Mozhgan Afshari** ³ and **Sónia A. C. Carabineiro** ^{4,*}¹ Department of Chemistry, Presidency University, Rajanukunte, Itgalpura, Bangalore 560064, Karnataka, India; anjaneyulu.bendi@gmail.com² Department of Chemistry, Faculty of Science, Baba Mastnath University, Rohtak 124001, Haryana, India; hit.ravirana@gmail.com³ Department of Chemistry, Shoushtar Branch, Islamic Azad University, Shoushtar, Iran; m.afshari@iau-shoushtar.ac.ir⁴ LAQV-REQUIMTE, Department of Chemistry, NOVA School of Science and Technology, Universidade NOVA de Lisboa, 2829-516 Caparica, Portugal

* Correspondence: versha2195@gmail.com (V); sonia.carabineiro@fct.unl.pt (S.A.C.C.)

Abstract: One of the most significant challenges the world is currently facing is wastewater treatment. A substantial volume of effluents from diverse sources releases numerous pollutants into the water. Among these contaminants, organic pollutants are particularly concerning due to the associated risk of being released into the environment, garnering significant attention. Rapid advancements in agriculture and industry on a global scale generate vast volumes of hazardous organic compounds, which eventually find their way into natural systems. Recently, the release of industrial wastewater has been increasing, due to the progress of numerous businesses. This poses a danger to humans and the environment, leading to environmental contamination. The application of carbon nanocomposites in applied nanotechnology has recently expanded due to their large surface area, substantial pore volume, low preparation cost, and environmental resilience. Expanding the use of nanomaterials in water treatment is essential, as magnetic carbon nanocomposites consistently demonstrate an efficient elimination of pollutants from water solutions. In the current study, we have highlighted the application of magnetic porous carbon nanocomposites in removing organic pollutants from wastewater.

Keywords: magnetic carbon nanocomposites; pollutants; adsorption; wastewater

Citation: Anjaneyulu, B.; Rana, R.; Versha; Afshari, M.; Carabineiro, S.A.C. The Use of Magnetic Porous Carbon Nanocomposites for the Elimination of Organic Pollutants from Wastewater. *Surfaces* **2024**, *7*, 120–142. <https://doi.org/10.3390/surfaces7010009>

Academic Editors: Shouzhong Zou and Irene Groot

Received: 31 December 2023

Revised: 2 February 2024

Accepted: 6 February 2024

Published: 21 February 2024



Copyright: © 2024 by the authors. Licensee MDPI, Basel, Switzerland. This article is an open access article distributed under the terms and conditions of the Creative Commons Attribution (CC BY) license ([https://creativecommons.org/licenses/by/4.0/](https://creativecommons.org/licenses/by/)).

1. Introduction

Wastewater reclamation or reuse has become an imperative need in the current scenario, given the rapid depletion of freshwater supplies. Agriculture alone accounts for 92% of global water usage [1–5], with approximately 70% of freshwater from rivers and subsurface sources dedicated to irrigation. This alarming statistic raises serious concerns for nations struggling with water scarcity [6–9]. Therefore, incorporating wastewater recycling in agriculture emerges as a pivotal strategy to substitute the use of freshwater [10].

In general, treated wastewater finds its application in various non-potable uses, including firefighting, vehicle washing, toilet flushing, irrigation, groundwater replenishment, golf course irrigation, building construction [11–16], and even for cooling purposes in thermal power plants. Both domestic water and treated wastewater contain a range of nutrients, such as nitrogen, phosphorus, sulfur and potassium. Notably, a significant portion of the nitrogen and phosphorus in wastewater is readily absorbable by plants, making it a viable option for irrigation [17,18].

Currently, diverse conventional technologies for wastewater treatment have been devised, including membrane filtration [19,20], flocculation [21,22], coagulation [23], Fenton

reagent [24,25], electrolysis [26] and photocatalytic oxidation [27]. Among the various available technologies, the adsorption method is acknowledged as a more cost-effective, efficient, practical and environmentally friendly alternative for wastewater treatment [28–30]. Various adsorbents have been examined for their effectiveness in purifying wastewater, including zeolites [31–33], clay minerals [34,35], kaolinite [36–38], pillared clays [39,40], silica gel [41,42], activated carbon [43–45] and biomass [46–48]. However, many existing adsorbents exhibit limited efficiency in removing specific contaminants in water, such as heavy metals and oil [49,50]. Numerous studies have emphasized the capability of activated carbon as an important adsorbent for the treatment of wastewater, owing to its significant porosity and expansive surface area [51–53].

The increased focus on nanotechnology has sparked a notable surge in the application of nanostructured materials across various domains, particularly in environmental remediation and wastewater treatment [54–56]. Nanostructured materials have particle sizes below 100 nm. They appear in diverse forms, including nanoparticles, nanotubes, nanowires and nanofibers [57–59]. Nanomaterials demonstrate superior adsorption abilities for various water contaminants when compared to larger bulk materials [60–62].

Carbon-based nanomaterials (CNMs) have garnered substantial attention as cutting-edge materials across various applications within the spectrum of nanostructured materials. This increased attention is due to their remarkable physical and chemical traits, alongside outstanding thermal, mechanical and electrical conductive characteristics [63–65]. The remarkable attributes of CNMs represent a significant advancement in technology, finding applications in diverse fields such as biosensors [66,67], reinforcing composite materials [68,69], materials with electrical conductivity [70], drug delivery [71,72], the biomedical field [73] and catalyst support [74,75]. Additionally, CNMs are widely acknowledged for their efficacy as superior adsorbents in wastewater pollutant removal [76–78].

Recently, there has been a growing interest in magnetic nanoparticles (NPs) in various environmental engineering applications. Spanning sizes between 1 and 100 nm and featuring a notable ratio of surface area to volume, with a capacity for carrying a high load, these nanoparticles have shown to be efficient materials used to trap pollutants from polluted water [79,80].

Despite the efficient adsorption capacity exhibited by carbon nanomaterials, their practical use faces challenges due to their strong adaptability and hydrophilic nature, complicating their retrieval and separation from water [81]. Separation using magnets emerges as a swift and efficient post-adsorption technique, surpassing alternatives like filtration and centrifugation [82]. Consequently, using Fe oxide nanoparticles for adsorption has attracted considerable interest. Besides their adsorption ability, these nanomaterials are cost effective, abundant and environmentally friendly. However, their inherent reactivity, especially in nanoparticle form, necessitates stability achieved through surface coating [83].

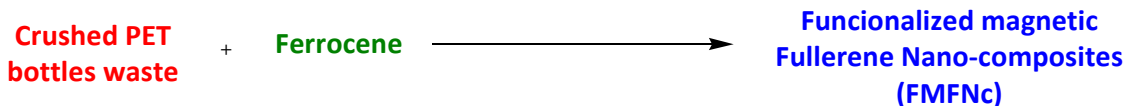
Recent findings reveal that it is possible to enhance the removal of organic dyes by coating magnetic iron oxide nanoparticles with carbon materials, facilitating easy recovery and recycling due to the synergistic impact of Fe oxides and carbon nanomaterials [84]. These altered materials have shown effectiveness in eliminating a range of dyes, like Rhodamine B (RhB) [85], methylene blue (MB), food yellow, and various others.

This review offers a comprehensive summary of magnetic porous carbon nanocomposites (magnetic fullerene, magnetic carbon dots, magnetic carbon nanotubes, magnetic graphite, magnetic graphene, and magnetic graphene oxide) for eliminating organic pollutants from wastewater. This data will contribute to advancing the rational design of magnetic porous carbon nanocomposites for water treatment, thereby contributing to the development of improved technologies for ensuring adequate water quality. Magnetic porous carbon nanocomposites can also be used for the removal of heavy metals. The interested reader should consult relevant reviews on the subject [86,87].

2. The Application of Magnetic Porous Carbon Nanocomposites

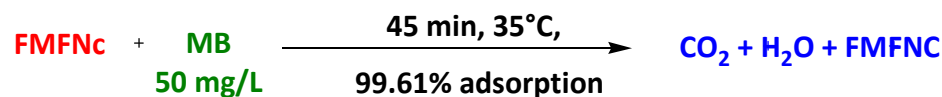
2.1. Magnetic Fullerene Nanocomposites

Elessawy et al. obtained magnetic fullerene nanocomposites with functionalization (FMFNC) in a simple, one-step and environmentally friendly manner. The method involved utilizing the catalytic thermal breakdown of waste PET bottles as a starting material and employing ferrocene both as a catalyst and as a source of magnetic nanoparticles in combination for eliminating MB and acid blue 25 (AB25) dyes through an adsorption process (Scheme 1). Subsequently, the composite could be effortlessly isolated using an external magnet [88].



Scheme 1. Synthesis of FMFNC.

After 10 consecutive cycles, FMFNC showed impressive effectiveness in adsorbing MB or AB25. The adsorption mechanism was verified through an examination of surface chemistry both prior to and following adsorption. It was primarily achieved through hydrogen bonding, π - π stacking contact, and electrostatic interaction. The advantages of high adsorption capacity and convenient separation are combined when fullerene and magnetic nanoparticles are used (Schemes 2 and 3).

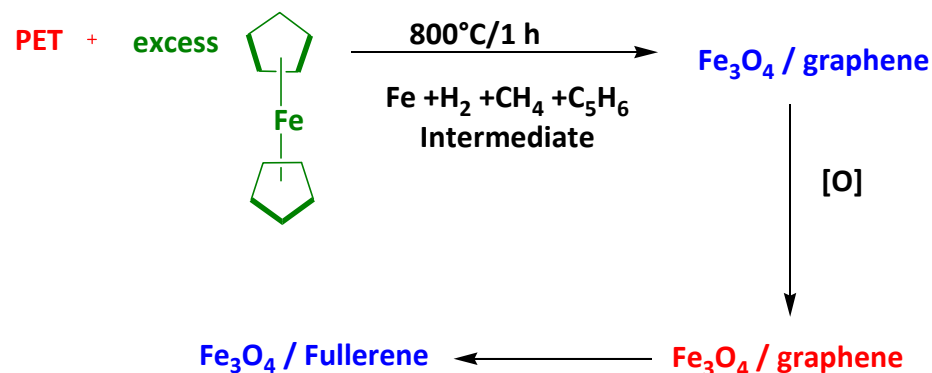


Scheme 2. Removal of methylene blue.

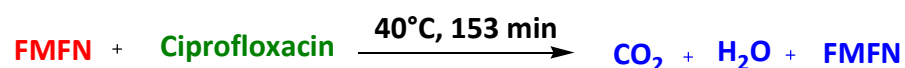


Scheme 3. Removal of acid blue 25.

Elessawy et al. obtained a new, simple, single-step method employed to produce functionalized magnetic fullerene nanocomposites (FMFN) by utilizing ferrocene both as a catalyst and a precursor for magnetite, along with the thermal catalytic decomposition of discarded poly(ethylene terephthalate) bottles as the source material [89] (Schemes 4 and 5).



Scheme 4. Synthesis of fullerene.

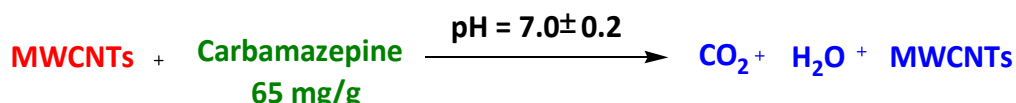


Scheme 5. Removal of ciprofloxacin.

According to the resolved equation, achieving the complete removal of ciprofloxacin requires optimal conditions: a contact time of 153 min and a ciprofloxacin amount of 65 mg/L at 40 °C. The spontaneity, exothermicity and increased casualness of the ciprofloxacin adsorption are confirmed by the negative ΔG and ΔH values, along with a positive ΔS value.

2.2. Magnetic Carbon-Dot Nanocomposites

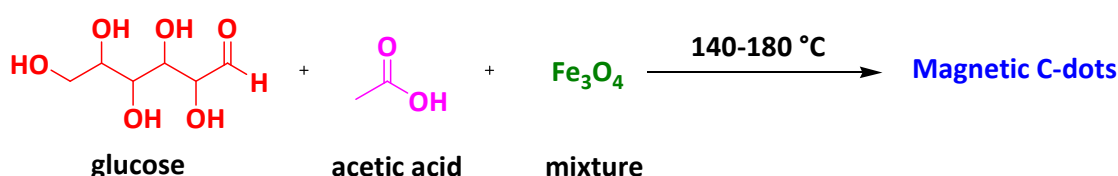
Deng et al. developed a procedure for creating carbon nanotubes (CNTs) modified with carbon dots (CMNTs) in three sequential steps: firstly, preparing magnetic carbon nanotubes; secondly, synthesizing carbon dots; and lastly, modifying the magnetic multiwalled carbon nanotubes surfaces using these carbon dots for the removal of carbamazepine [90] (Scheme 6).



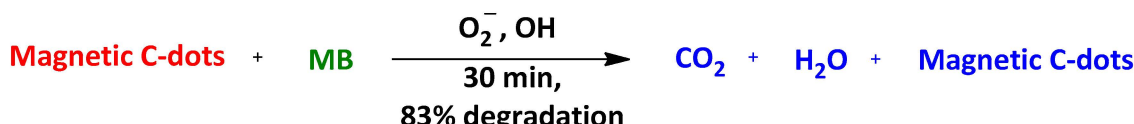
Scheme 6. Removal of carbamazepine.

At a pH of 7.0 ± 0.2 , CMNTs showed a substantial adsorption of 65 mg/g, surpassing that of numerous previously documented adsorbents. The removal of carbamazepine by CMNTs showed swift removal within the initial 3 h, with kinetics effectively modeled by the HSDM and pseudo-second-order models. The simplified HSDM model effectively characterizes the declining adsorption capacity of CMNTs over time and illustrates the movement of carbamazepine particles within the CMNTs. The material used for adsorption can undergo regeneration and be reused repeatedly, experiencing a capacity reduction of less than 2.2% across six cycles.

Sun created magnetic carbon dots by combining C-dots with magnetic Fe_3O_4 nanoparticles. This synthesis aimed to investigate their photocatalytic performance in the presence of visible light and assess their recyclability in wastewater treatment. The specimens were created using a bottom-up method at a reaction temperature (T_r) set at 140 °C and 180 °C, with various reaction times ($t_r = 0\text{--}18$ h). The outcomes revealed a progressive attachment of C-dots to Fe_3O_4 nanoparticles as t_r increased at $T_r = 140$ °C, while a sudden move towards the maximum adsorption on Fe_3O_4 occurred at $T_r = 180$ °C [91] (Schemes 7 and 8).



Scheme 7. Synthesis of magnetic C-dots.



Scheme 8. Removal of methylene blue.

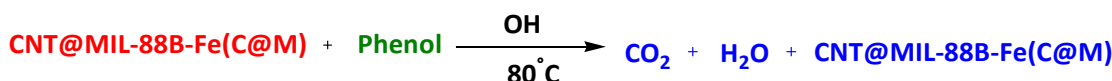
In just half an hour of exposure to visible light, the MB amount can decrease by 83%. The recyclability experiment distinctly indicated that the magnetic C-dots exhibited the capability for over a tenfold increase in photocatalytic degradation.

2.3. Magnetic Carbon Nanotube Nanocomposites

Zhang et al. developed a remarkably effective Fenton-like catalyst for breaking down organic pollutants by synthesizing MIL-88B-Fe with integrated CNTs. The latter possess

surface oxygen functional groups rich in electrons. CNTs were integrated into the metal-organic framework to enhance Fe(II) content, thereby improving Fenton-like behavior. The synthesized CNT@MIL-88B-Fe (C@M) exhibited significantly enhanced catalytic capabilities.

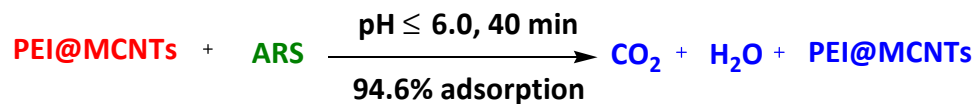
The rate constant for the pseudo-first-order kinetics of phenol elimination using C@M (0.32 min^{-1}) surpassed that of MIL-88B-Fe by approximately sevenfold and rivaled or exceeded values reported for other heterogeneous Fenton-like materials. Furthermore, the Fenton-like system demonstrated an effective degradation of diverse persistent organic contaminants and showcased remarkable catalytic activity across a broad pH spectrum (4–9). XPS verified a gradual increase in the Fe(II) amount of the catalyst with CNT loadings [92] (Scheme 9).



Scheme 9. Removal of phenol.

Zhang et al. successfully synthesized an adsorbent of magnetic CNTs functionalized with polyethyleneimine (PEI@MCNTs) and thoroughly examined its adsorption capacity to eliminate Alizarin Red S (ARS) from the dyeing effluent. PEI@MCNTs were made using the co-precipitation technique.

ARS could be effectively extracted from an acidic aqueous solution ($\text{pH} \leq 6.0$) using PEI@MCNTs for 40 min at an ambient temperature. Thanks to their numerous contacts and abundance of adsorption sites, PEI@MCNTs exhibited a spontaneous adsorption process and good selectivity towards ARS. PEI@MCNTs had the highest adsorption capacity of 196.08 mg g^{-1} for ARS, as obtained by the Langmuir isotherm. The efficiency of removing ARS in tap, river and lake waters stayed within the range of 94.6%, 89.3%, and 91.8%, respectively, closely resembling the efficiency observed in distilled water (96.7%). This capacity exceeded that of conventional adsorbents currently on the market. Additionally, the PEI@MCNTs were easily regenerated using a 10 mM NaOH solution after being collected using an external magnet. The PEI@MCNTs prepared exhibit promise as adsorbents for efficiently removing anthraquinone dyes in extensive wastewater treatment [93] (Scheme 10).



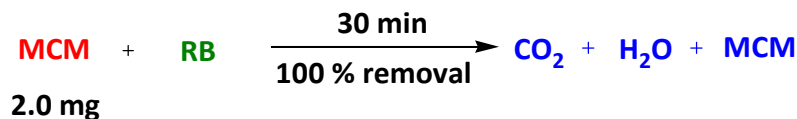
Scheme 10. Removal of Alizarin Red S.

Salam et al. developed a composite containing multi-walled carbon nanotubes (MWCNTs), magnetite and chitin, creating a magnetic nanocomposite with the purpose of efficiently eliminating Rose Bengal from both authentic and simulated solutions [94]. This magnetic nanocomposite was formed by physically combining MWCNTs with the biopolymer chitin and magnetite.

Various factors influencing the removal of Rose Bengal using an MCM nanocomposite were explored. The findings indicated that increasing the mass of MCM improved the adsorption process, with the optimal removal of Rose Bengal being achieved using 2 mg of MCM. Furthermore, the impact of adsorption time was investigated, revealing that equilibrium in adsorption was obtained after 30 min. The findings suggested that adsorption adhered to the pseudo-second-order kinetic model.

The outcomes revealed that the extraction of Rose Bengal from a water solution by an MCM composite was physically driven and endothermic. This was clear from the increased adsorption capability with rising solution temperature. Moreover, the negative ΔG , along with the positive ΔH and ΔS values, indicate that the adsorption of Rose Bengal is driven by entropy. When applied to remove Rose Bengal from an artificially contaminated wastewater

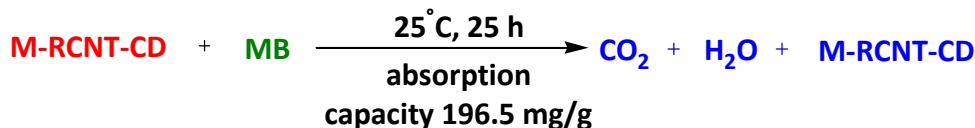
sample, the MCM nanocomposite exhibited nearly 100% removal and retained its efficiency over five consecutive cycles (Scheme 11).



Scheme 11. Removal of Rose Bengal.

Cheng et al. developed a method to create composites of β -cyclodextrin (CD) attached to CNTs using cyclodextrins (CDs) and conducted reduction with the hydrazine hydrate of oxidized CNT. The resulting reduced samples (RCNT-CD) were affixed to Fe oxide during the creation of magnetic analogs (M-RCNT-CD).

M-RCNT-CD demonstrated a maximal adsorption of 196.5 mg/g of MB. The negative change in ΔG° and the positive change in ΔH° indicate that adsorption is spontaneous and endothermic, respectively; thus, the magnetic adsorbent is efficient for the removal of organic contaminants from water solutions [95] (Scheme 12).



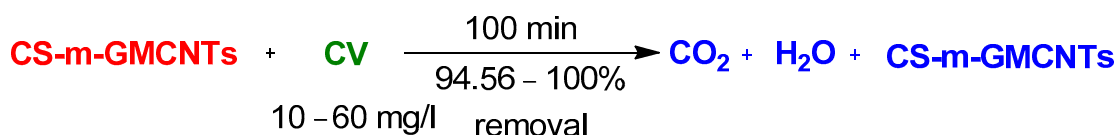
Scheme 12. Removal of methylene blue.

Zhu et al. synthesized magnetic graphitized MWCNTs modified with chitosan (CS-m-GMCNTs) using a cross-linking suspension method. The structure, form and magnetic characteristics of the synthesized CS-m-GMCNTs were assessed through several characterization techniques.

The model representing second-order kinetics, exhibiting high correlation coefficients ($R^2 > 0.998$), proved to be appropriate for characterizing the rate at which crystal violet is adsorbed onto CS-m-GMCNTs. A color removal of up to 94.58% and 100% was attainable within 100 min for water solutions of 10 and 60 mg L⁻¹, respectively.

Magnetic tests showed that CS-m-GMCNTs could attain a saturated magnetization of 12.27 emu g⁻¹. Additionally, the adsorption capability of crystal violet on CS-m-GMCNTs reached 263 mg g⁻¹. The thermodynamic parameter values suggested the adsorption had a significant reliance on the temperature of the liquid phase, suggesting a spontaneous and heat-releasing reaction.

Hence, CS-m-GMCNTs exhibit notable advantages, including very good dispersion in water, convenient separation and elevated adsorption capability. These characteristics suggest the possibility of its application in the efficient elimination of other carcinogenic and hazardous contaminants from water [96] (Scheme 13).

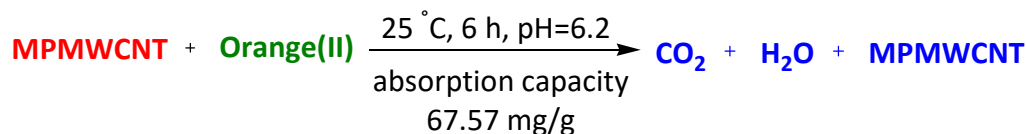


Scheme 13. Removal of crystal violet.

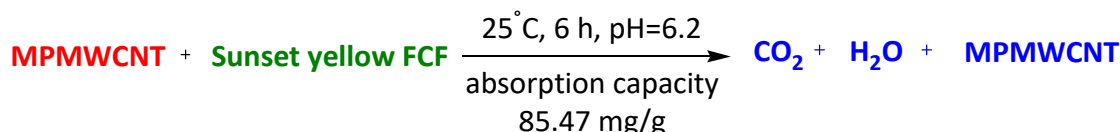
Gao et al. made a nanocomposite of magnetic polymer and MWCNTs to adsorb anionic azo dyes from water solutions.

The capturing capability of the magnetic polymer's multiwall carbon nanotube nanocomposite (MPMWCNT) was evaluated in solutions containing orange II, sunset yellow FCF and amaranth, and proved to be higher than that of magnetic MWCNTs without PGMIC. The adsorption capability sequence for anionic azo dyes was amaranth < orange II < sunset yellow

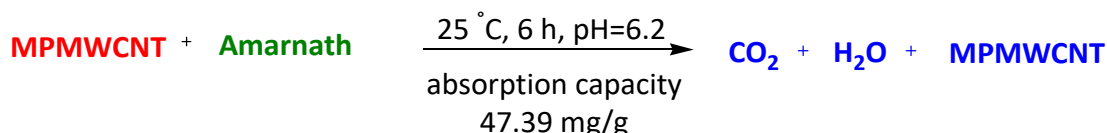
FCF. As the pH increased, the adsorption progressively diminished. The highest q_m values at 25 °C were 67.6, 85.5 and 47.4 mg g⁻¹ for orange II, sunset yellow FCF and amaranth, respectively [97] (Schemes 14–16).



Scheme 14. Removal of orange (II).



Scheme 15. Removal of sunset yellow FCF.

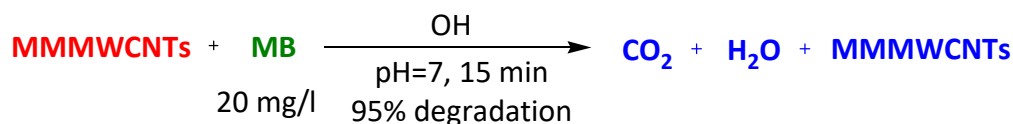


Scheme 16. Removal of amaranth.

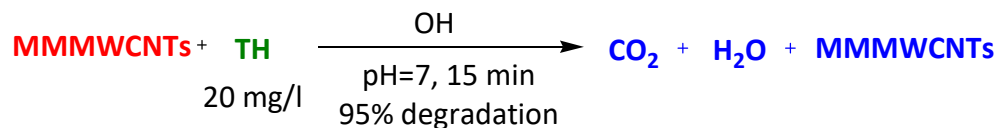
Madakian et al. focus on removing specific positively charged dyes from water using MWCNTs modified with magnets. MWCNTs loaded with Fe₃O₄ nanoparticles were synthesized through a straightforward solution-based approach. This involved the dissolving of ammonium iron (II) sulfate hexahydrate in water and a hydrazine hydrate solution (3:1 volume ratio), followed by the addition of pre-treated MWCNTs.

The best pH for eliminating all studied cationic dyes from water was 7.0. The highest anticipated adsorption amounts of CV, JG, Th and MB dyes were 228, 250, 36 and 48 mg g⁻¹, respectively. The desorption was additionally examined, employing acetonitrile as a solvent.

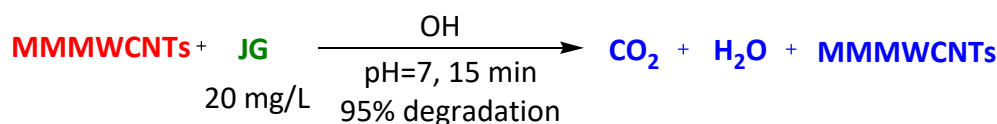
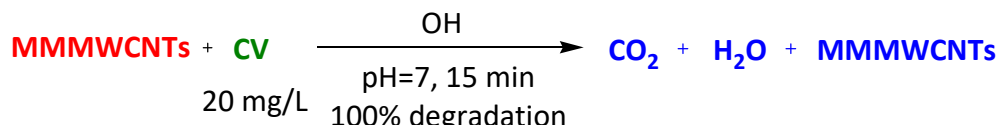
The variation in adsorption capability can be ascribed to distinctions in dye structures. JG and CV feature quaternary ammonium groups, while MB and Th are characterized as cationic sulfide dyes. The positive charge of JG and CV is distributed throughout the molecule, whereas in MB and Th, the positive charge accumulates around the heteroatom ring. Consequently, the adsorption of JG and CV onto the adsorbent proves more effective than that of MB and Th dyes. Maximum adsorption was achieved with 0.015 g of the adsorbent, resulting in approximately 95% removal for Th and MD and complete removal (100%) for JG and CV [98] (Schemes 17–20).



Scheme 17. Degradation of methylene blue.

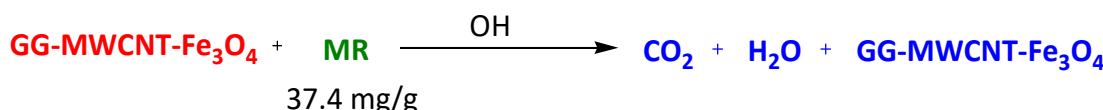
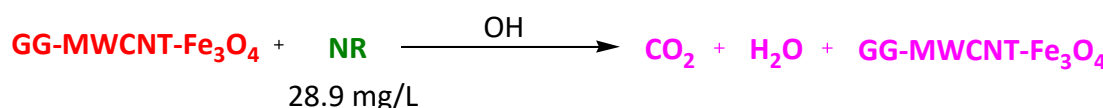


Scheme 18. Degradation of Thioflavin.

**Scheme 19.** Degradation of Janus Green.**Scheme 20.** Degradation of crystal violet.

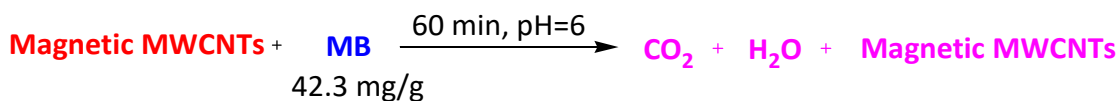
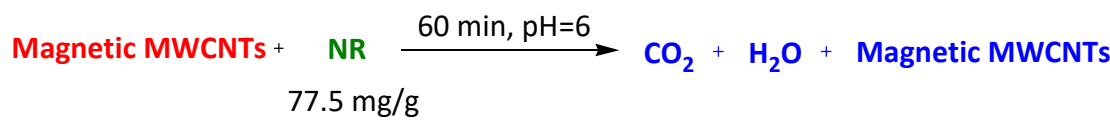
Yan et al. created magnetic carbon nanotubes modified with guar gum for the purification of wastewater. Magnetic GG–MWCNT–Fe₃O₄ was synthesized by suspending GG–MWCNT in a solution containing FeCl₃ and FeSO₄ at 60 °C under a N₂ atmosphere. A solution of NH₃ was added, adjusting the mixture's pH between 10 and 11.

The isotherms showed that adsorption followed the Langmuir model, with GG–MWCNT–Fe₃O₄ exhibiting maximal adsorption of 61.9 mg g⁻¹ for MB and 89.9 mg g⁻¹ for NR. The magnetic GG–MWCNT–Fe₃O₄ demonstrates magnetic separation and adsorption capacity properties, making it a viable choice for eliminating pollutants from aqueous solutions [99] (Schemes 21 and 22).

**Scheme 21.** Degradation of methylene blue.**Scheme 22.** Degradation of methylene blue.

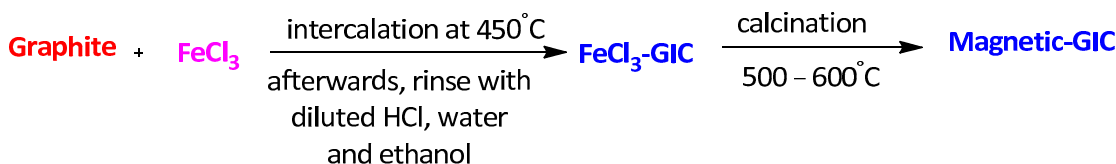
Qu et al. fabricated MWCNTs filled with Fe₂O₃ particles to eliminate organic dyes from contaminated water. MWCNTs loaded with γ-Fe₂O₃ nanoparticles were synthesized through a hydrothermal reaction involving MWCNTs in a ferric nitrate solution, followed by calcination.

The dye adsorption test, involving neutral red (NR) and MB, reveals that equilibrium is reached within just 60 min. At pH 6, the adsorption capacities within the tested concentration span are 77.5 mg/g for NR and 42.3 mg/g for MB, making magnetic MWCNTs function as outstanding absorbents for these dyes. Unlike other materials, magnetic nanotubes not only demonstrate superior efficacy in dye adsorption but also offer convenient manipulation through an external magnetic field [100] (Schemes 23 and 24).

**Scheme 23.** Removal of methylene blue.**Scheme 24.** Removal of neutral red.

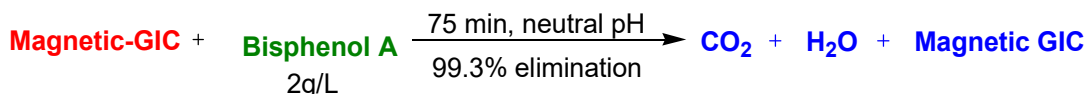
2.4. Magnetic Graphite Nanocomposites

Ranjbar et al. synthesized magnetic graphite intercalation components as persulfate activators for Bisphenol A elimination from wastewater at pH 7. The “molten salt method” was employed to manufacture FeCl_3 -GIC followed by calcination to generate magnetic GIC [101] (Scheme 25).



Scheme 25. Synthesis of magnetic-GIC.

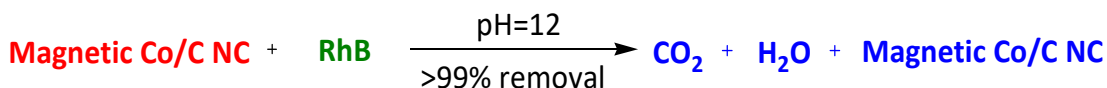
With 2 g/L of catalyst and 1.2 g/L of persulfate at pH 7, the suggested method eliminated 99.3% of BPA in 75 min. Quenching assays revealed that the catalytic activity and removal of BPA were boosted by the production of free radicals and singlet oxygen, occurring through radical and non-radical routes. Additionally, the potential of recycling the manufactured catalyst was explored by its application to treated city wastewater. The findings indicated that the catalyst was capable of breaking down BPA in the wastewater in successive cycles, indicating its practicality (Scheme 26).



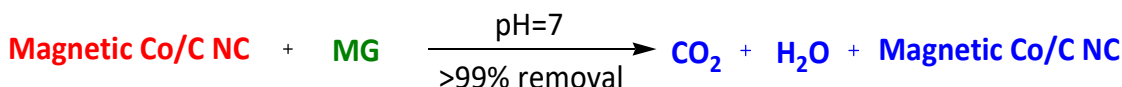
Scheme 26. Removal of Bisphenol A.

Ruan C. P et al. developed a Co/C magnetic nanocomposite resistant to acid by employing ZIF-67 as a template and precursor [102]. It underwent carbonization in the Ar atmosphere, followed by acid treatment. Through calcination in an inert atmosphere, Co nanoparticles formed and were evenly enveloped by graphite layers, facilitated by the catalytic effect of the Co-induced graphitization of carbon. These graphite layers protected against oxidation and acidic environments for the Co particles. Consequently, an acid-resistant magnetic adsorbent was created, suitable for application in a broad pH range (pH 1–13).

The magnetic Co/C, produced through synthesis, exhibited outstanding adsorption performance for two common dyes (RhB and malachite green, MG) across a broad pH spectrum, achieving a removal efficiency exceeding 99%. The adsorption behavior of these dyes was accurately explained by the Langmuir model in the adsorption isotherms. Notably, the maximum adsorption capacities for RhB and MG were 400.0 and 561.8 mg g⁻¹, respectively, surpassing the capacities of several mentioned adsorbents. Additionally, the adsorbent could be effortlessly regenerated through washing with ethylene glycol (EG), indicating remarkable reusability. After undergoing five reuse cycles, there was no observable decline in capacity. Moreover, the magnetic adsorbent demonstrated its practical use by attaining a removal efficiency surpassing 97% in eliminating organic dyes from household wastewater (Schemes 27 and 28).

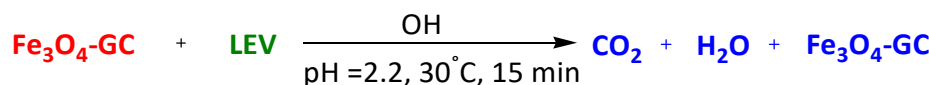


Scheme 27. Removal of Rhodamine B.



Scheme 28. Removal of malachite green.

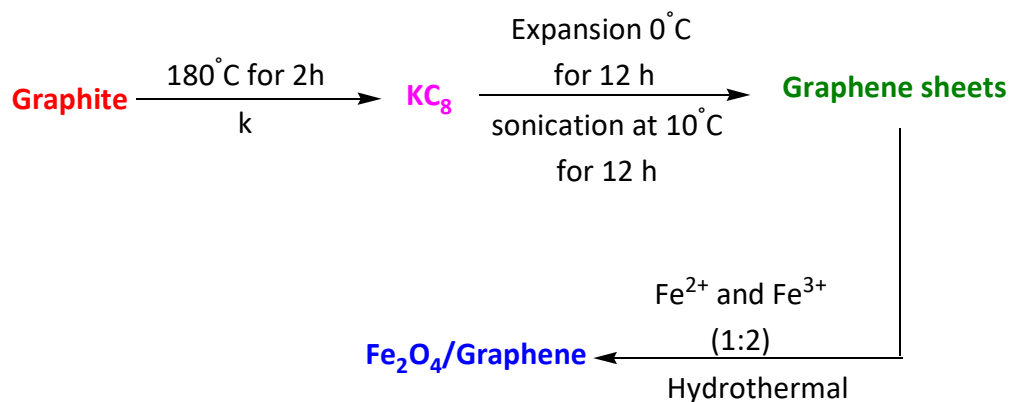
Wang et al. produced a Fe_3O_4 -graphite composite, which was synthesized, characterized and explored as a Fenton-like heterogeneous catalyst for levofloxacin (LEV) degradation in water. The composite was produced through a solvothermal one-step method and displayed remarkable characteristics for the elimination of LEV, accomplishing almost full elimination of 50 mg L^{-1} LEV within 15 min and 48% removal of total organic carbon in 60 min. The extensive conjugation electronic structure present in graphite might facilitate the rapid generation of OH^\bullet radicals due to the facile reduction of Fe^{3+} to Fe^{2+} . Furthermore, it was noted that graphite could degrade LEV in H_2O_2 . Hence, the combined effects of the graphitic structure and Fe_3O_4 MNPs likely promote the elevated catalytic activity of the composite. The efficiency of LEV degradation remained at ~80% during the fifth recycle, highlighting the potential applications of the material in water treatment for the removal of organic pollutants [103] (Scheme 29).



Scheme 29. Degradation of levofloxacin.

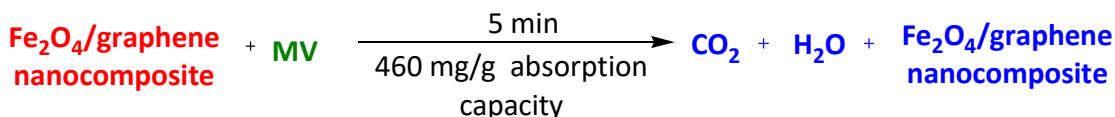
2.5. Magnetic Graphene Nanocomposites

Bharath et al. conducted studies focused on creating magnetite on porous graphene-based nanocomposites for novel adsorption and electrosorption techniques aimed at removing organic pollutants from wastewater. Initially, porous graphene was dispersed in water using ultrasonication. The resulting supernatant was collected. Subsequently, solutions of FeCl_2 and FeCl_3 were added, maintaining a pH range of 10–11 by introducing an ammonium hydroxide solution. After being kept at 180°C for 12 h, it was washed with ethanol [104] (Scheme 30).



Scheme 30. Synthesis of Fe_2O_4 /porous graphene nanocomposites.

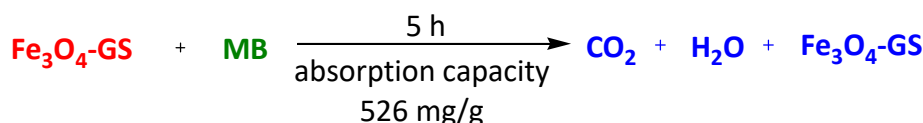
The adsorption capacities of dyes were notably high in the case of Fe_3O_4 /porous graphene nanocomposites. The adsorption of Fe_3O_4 on porous graphene was tested using methyl violet as an adsorbate. Fe_3O_4 /porous graphene demonstrated swift adsorption within 5 min, possessing a high adsorption capability (Q_0 –60 mg/g) and facilitating convenient separation and recyclability. This is ascribed to the elevated surface area resulting from the porosity of graphene and the strong magnetic properties of Fe_3O_4 (Scheme 31).



Scheme 31. Removal of methyl violet.

Yu et al. developed a magnetic sponge of graphene (Fe_3O_4 -GS) designed for the elimination of MB. Fe_3O_4 -GS was synthesized through lyophilization to facilitate the adsorption of dyes. Fe_3O_4 -GS showed impressive adsorption of 526 mg/g for MB, exceeding the values reported for magnetic carbon nano-adsorbents in the existing literature. The kinetics of the adsorption of MB on Fe_3O_4 -GS displayed a rapid rate, amenable to analysis through the pseudo-second-order and intraparticle diffusion models. The thermodynamic parameters indicate that, when feasible, the adsorption of MB on Fe_3O_4 -GS should be conducted at elevated temperatures.

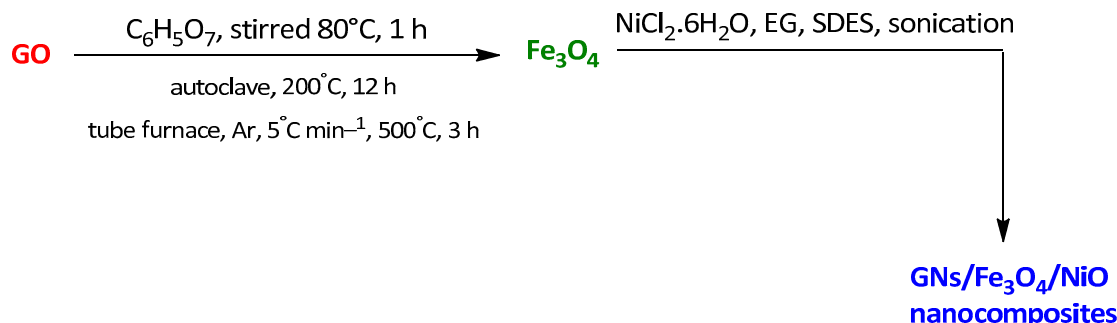
The thermodynamic investigation unveiled that the adsorption process was motivated by enhanced interface randomness. Additionally, both pH and ionic strength significantly impacted the adsorption capability of Fe_3O_4 -GS [105] (Scheme 32).



Scheme 32. Removal of methyl blue.

Zhao et al. synthesized a novel magnetic photocatalyst of graphene with Fe_3O_4 and NiO (GNs/ Fe_3O_4 /NiO), through a straightforward method. Three types of nanocomposites were produced with varying NiO contents: 50% (S1), 67% (S2) and 75% (S3), by weight.

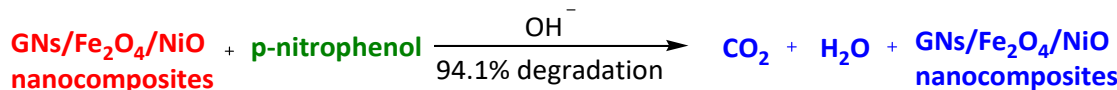
The resulting mixture of GNs/ Fe_3O_4 , NiO MNPs and dodecyl benzene sulfonic acid sodium (SDBS) were sonicated in ethylene glycol and stirred at 25 °C in N_2 for 24 h, after which the product was isolated from the solution using a magnetic field. After washing with ethanol, GNs/ Fe_3O_4 /NiO nanocomposites were obtained [106] (Scheme 33).



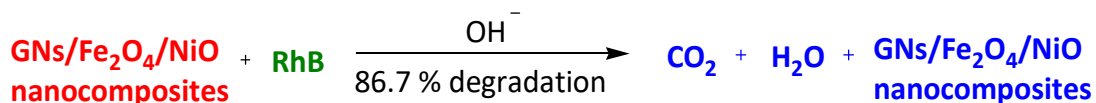
Scheme 33. Synthesis of GNs/ Fe_3O_4 /NiO nanocomposites.

The experimental findings indicated a notable improvement in both magnetic and adsorption performance for magnetic GNs/ Fe_3O_4 /NiO nanocomposites. The saturation magnetizations for the three types of nanocomposites, GNs/ Fe_3O_4 /NiO (S1), GNs/ Fe_3O_4 /NiO (S2) and GNs/ Fe_3O_4 /NiO (S3), were approximately 63.1, 43.3 and 22.4 emu g⁻¹, respectively.

The nanocomposites demonstrated elevated photocatalytic ability towards p-nitrophenol and RhB. Additionally, the degradation rate of S3 nanocomposites for p-nitrophenol and RhB were approximately 94.1% and 86.7%, respectively. Even after three uses, the degradation rate of S3 for p-nitrophenol and RhB remained above 90% and 84%, respectively. This suggests that the nanocomposites exhibit robust photocatalytic performance and hold significant potential for future applications in the field of photocatalysis (Schemes 34 and 35).

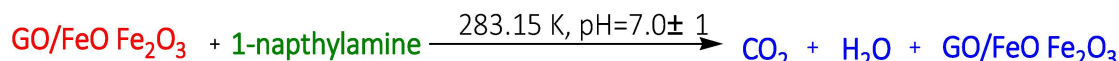
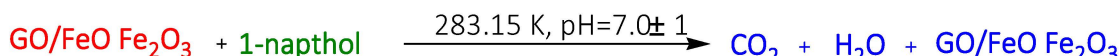
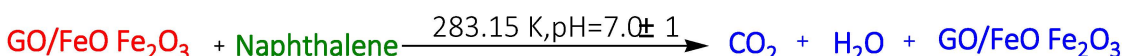


Scheme 34. Degradation of p-nitrophenol.

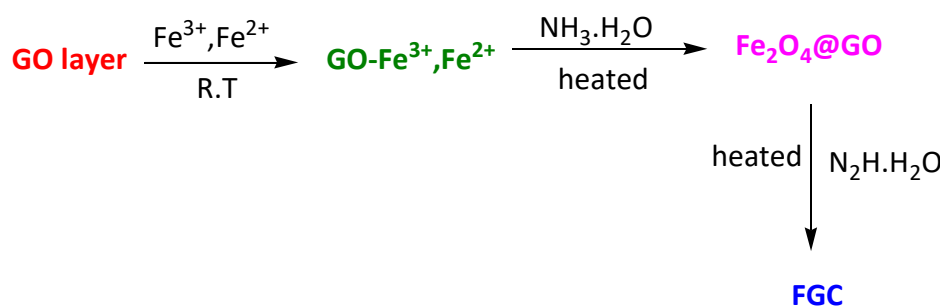
**Scheme 35.** Degradation of Rhodamine B.

Yang et al. synthesized super adsorbents by creating reduced graphene oxide (GO) on Fe oxide ($\text{GO}/\text{FeO}\bullet\text{Fe}_2\text{O}_3$) for the adsorption of 1-naphthylamine, 1-naphthol and naphthalene with distinct polarities. GO was produced using a modified Hummers method from graphite flakes. Magnetic composites were formed through co-precipitation involving ferrous and ferric ions on the surfaces of GO or MWCNTs.

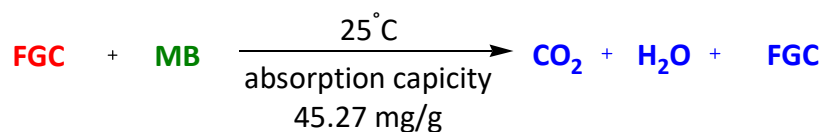
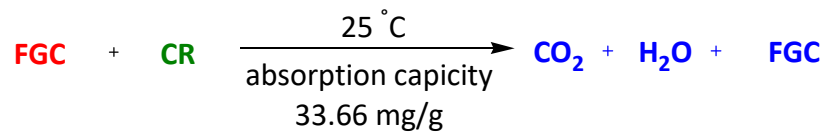
The adsorption followed the following order: 1-naphthylamine > 1-naphthol > naphthalene. The mechanism proposed was the electron donor–acceptor (EDA) interaction, with the adsorptive capability rising with an increase in dipole moment. In contrast to the combination of MWCNTs and iron oxide (MWCNTs/ $\text{FeO}\bullet\text{Fe}_2\text{O}_3$), we observed that the structure of the adsorbents significantly influenced the adsorption of these aromatic compounds [107] (Schemes 36–38).

**Scheme 36.** Removal of 1-naphthylamine.**Scheme 37.** Removal of 1-naphthol.**Scheme 38.** Removal of naphthalene.

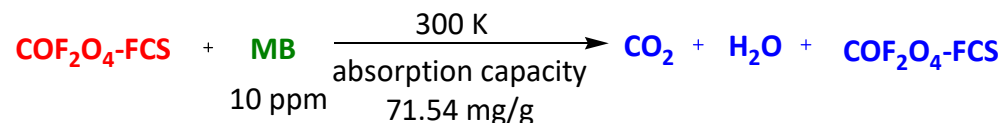
The synthesis procedure for the magnetic composite $\text{Fe}_3\text{O}_4@\text{graphene}$ (FGC) involved the following steps: GO was dispersed in water through sonication to convert carboxylic acid groups into carboxylate anions. Subsequently, a solution of FeCl_3 and FeCl_2 was added to the GO suspension at 25 °C under N_2 with stirring. Following the ion exchange process, an ammonia solution was introduced dropwise to adjust the solution's pH to 10 for the synthesis of magnetite Fe_3O_4 nanoparticles [108] (Scheme 39).

**Scheme 39.** Synthesis of FGC.

The adsorption of MB and Congo Red (CR) on the $\text{Fe}_3\text{O}_4@\text{graphene}$ composite (FGC) was studied in batch. FGC demonstrated maximum adsorption capacities of 45.3 mg/g for MB and 33.7 mg/g for CR. The sorption kinetics were represented by the second-order kinetic equation (Schemes 40 and 41).

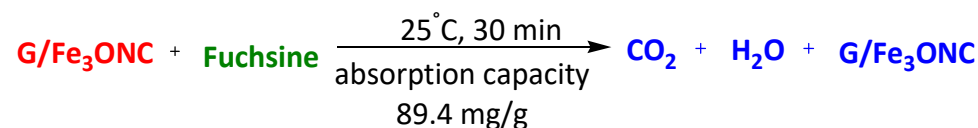
**Scheme 40.** Removal of methylene blue.**Scheme 41.** Removal of Congo Red.

Li et al. obtained nanocomposites of magnetic CoFe_2O_4 functionalized graphene sheets (CoFe_2O_4 -FGS) hydrothermally treating inorganic salts and thermally exfoliating graphene sheets. For studying the adsorption of CoFe_2O_4 -FGS, the model compound chosen was the common contaminant methyl orange (MO). The CoFe_2O_4 -FGS with magnetic separation capability showed significant adsorption ability (71.54 mg g^{-1}) for MO molecules, starting from 10 ppm. This suggests that CoFe_2O_4 -FGS could be advantageous for applications related to separation and purification [109] (Scheme 42).

**Scheme 42.** Removal of methyl blue.

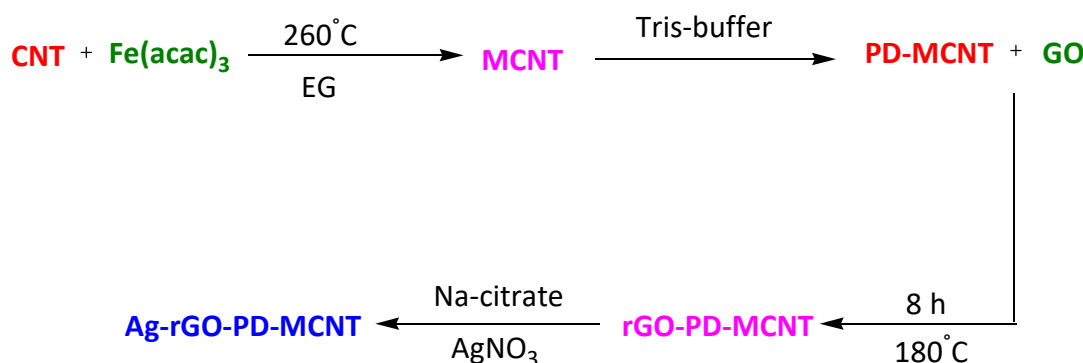
Wang et al. produced a graphene-based magnetic nanocomposite ($\text{G}/\text{Fe}_3\text{O}_4$) and utilized it to eliminate dye from water solutions. The synthesis of $\text{G}/\text{Fe}_3\text{O}_4$ involved the co-precipitation of Fe^{2+} and Fe^{3+} in alkaline conditions with graphene.

The adsorption process is rapid, achieving equilibrium within 30 min. The kinetic data were effectively modeled using a pseudo-second-order approach. Both Freundlich and Langmuir models were employed to analyze the isotherms. The collected data fitted a pseudo-second-order method. Even after undergoing five regenerations, the maximum amount of fuchsine that $\text{G}/\text{Fe}_3\text{O}_4$ can adsorb did not exhibit a notable decrease [110] (Scheme 43).

**Scheme 43.** Removal of fuchsine.

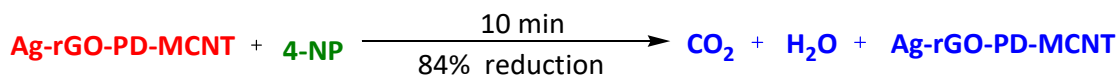
2.6. Magnetic Graphene Oxide Nanocomposites

Islam et al. introduced an innovative approach to creating a magnetic CNT-reduced GO (rGO) Ag nanocomposite. The Ag-rGO-PD-MCNT nanocomposite was created by reducing AgNO_3 in a rGO-PD-MCNT suspension using sodium citrate (Scheme 44).

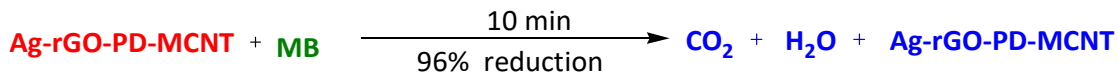


Scheme 44. Synthesis of Ag–rGO–PD–MCNT composite.

The synthesized nanocomposites exhibited significant catalytic efficacy alongside rapid and efficient adsorption, demonstrated across various pH levels during the elimination of a model 4-nitrophenol, MB and an aromatic nitro compound, toxic dye. Within 4 min, the absorbance at both wavelengths reached saturation and the distinctive yellow color of 4-nitrophenol almost completely disappeared, signifying an approximate 84% reduction. In the presence of the nanocomposites, the reduction of MB reached up to 96% within 10 min, resulting in the emergence of a colorless solution. The nanocomposites were magnetically isolatable, easily restored by desorption with water and ethanol, enabling their repeated use for over 15 cycles due to high recyclability [111] (Schemes 45 and 46).



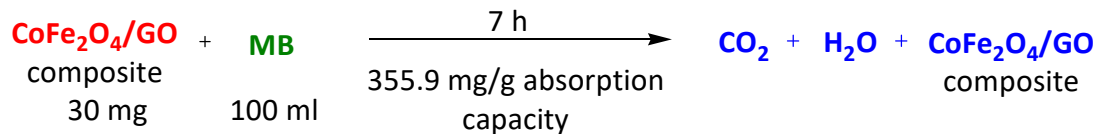
Scheme 45. Removal of 4-nitrophenol.



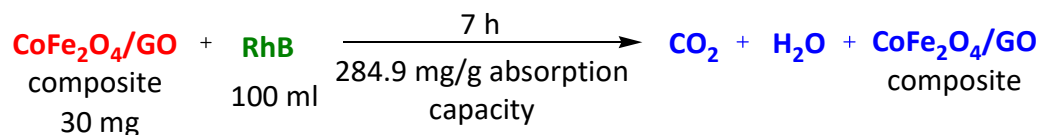
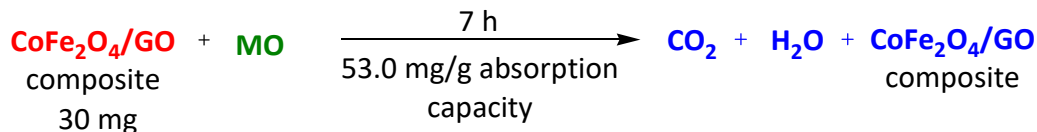
Scheme 46. Removal of methylene blue.

Chang et al. synthesized magnetic CoFe₂O₄/GO through a straightforward hydrothermal procedure. The structure, morphology and magnetic properties of the resulting materials were characterized using several techniques.

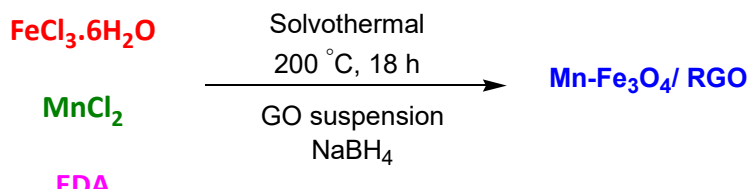
The CoFe₂O₄/GO composites were employed for removing RhB, MB and methyl orange (MO). Remarkably, there was minimal detection of adsorption for these three dyes on the initially synthesized CoFe₂O₄, validating that the adsorption capability of dyes on CoFe₂O₄/GO mainly arises from the presence and contribution of GO. A clear selective adsorption is observed, with the order being MO < RhB > MN. The Langmuir model reveals a remarkable adsorption of 355.9 mg/g for MB, 284.9 mg/g for RhB and 53.0 mg/g for MO. The presence of oxygenated groups in GO significantly influences its adsorption ability. The adsorption capacity is higher for carboxyl (–COOH) modifications on the GO surface compared to epoxy (–CH(O)CH–) or hydroxyl (–OH) species. This insight opens up a new avenue for designing adsorbent materials based on graphene oxide [112] (Schemes 47–49).



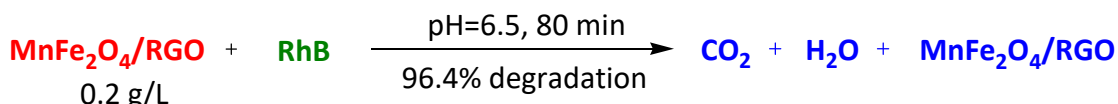
Scheme 47. Removal of methylene blue.

**Scheme 48.** Removal of Rhodanine B.**Scheme 49.** Removal of methyl orange.

Chen et al. developed an innovative hybrid, Mn-doped Fe_3O_4 hollow microspheres on rGO ($\text{Mn}-\text{Fe}_3\text{O}_4/\text{rGO}$), using a simple solvothermal method. This was followed by reducing GO through NaBH_4 [113] (Scheme 50).

**Scheme 50.** Synthesis of $\text{Mn}-\text{Fe}_3\text{O}_4/\text{RGO}$.

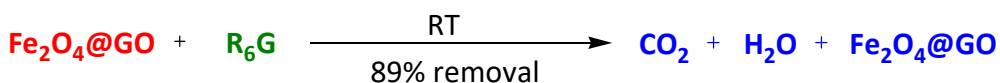
The $\text{Mn}-\text{Fe}_3\text{O}_4/\text{RGO}$ hybrid, produced in this manner, serves as a photo-Fenton material for RhB degradation, achieving a remarkable 96.4% efficiency with a minimal catalyst amount of 0.2 g/L. This happens when exposed to UV-visible light and with the presence of H_2O_2 at the ambient pH of around 6.5, all within an 80 min timeframe. Notably, removal efficiencies of 91% and 85% are observed at pH 11 and 2, respectively. Moreover, this innovative photo-Fenton material maintains a robust degradation of approximately 90% even after undergoing ten cycles (Scheme 51).

**Scheme 51.** Degradation of Rhodamine B.

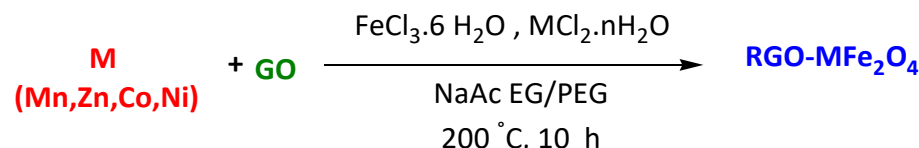
Mishra and Mohanty synthesized GO sheets decorated with Fe_3O_4 nanoparticles for the purpose of removing organic pollutants. $\text{Fe}_3\text{O}_4@\text{GO}$ nanocomposites were prepared by incorporating GO into double-distilled water through sonication. Subsequently, Fe_3O_4 powder was introduced into the solution, succeeded by ultrasonication. Ultimately, hydrazine hydrate was introduced into the blend, and then sonicated before undergoing centrifugation and subsequent washing [114] (Scheme 52).

**Scheme 52.** Synthesis of $\text{Fe}_3\text{O}_4@\text{GO}$.

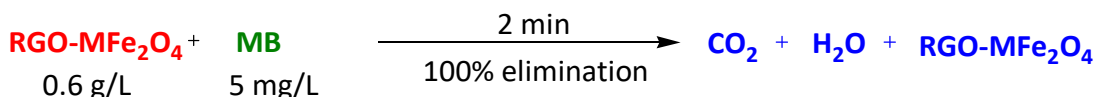
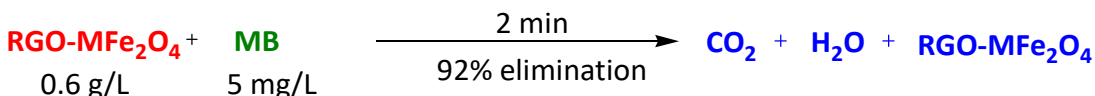
The $\text{Fe}_3\text{O}_4@\text{GO}$ nanocomposites exhibit superparamagnetic behavior, characterized by a magnetic saturation (MS) of 30.6 emu/g. Different concentrations of $\text{Fe}_3\text{O}_4@\text{GO}$ nanocomposites were used to remove R6G from a water-based solution. Achieving a removal of 89%, these results hold significance for environmental considerations, demonstrating that $\text{Fe}_3\text{O}_4@\text{GO}$ nanocomposites can effectively eliminate organic pollutants from water (Scheme 53).

**Scheme 53.** Removal of Rhodamine 6G.

Bai et al. introduced a single-pot solvothermal technique for crafting hybrids that incorporate reduced ferrite (MFe_2O_4 , $\text{M} = \text{Co}, \text{Mn}, \text{Ni}, \text{Zn}$) and rGO. The process involved utilizing metal and graphite oxide and ions (M^{2+} and Fe^{3+}) as initial components [115] (Scheme 54).

**Scheme 54.** Synthesis of RGO–MFe₂O₄.

The hybrids exhibit substantial saturation magnetization, along with reduced remanence and coercivity. Notably, these hybrids prove to be efficient adsorbents for eliminating dye pollutants. This shows that the hybrids can eliminate over 100% of MB and 92% of RhB with (5 mg/L) in 2 min, provided the hybrid concentration is 0.6 g/L (Schemes 55 and 56).

**Scheme 55.** Elimination of methylene blue.**Scheme 56.** Elimination of Rhodamine B.

Song et al. employed a single-step solvothermal technique to effectively create nanocomposites containing CoFe_2O_4 and reduced graphene oxide (CFG).

Due to favorable electrostatic interactions, CFG exhibits a significantly greater adsorption amount for anionic dyes in comparison to cationic dyes. The adsorption capacity for MO reaches a notable 263 mg g^{-1} at 25°C , with the isotherms conforming to the Langmuir model. Additionally, CFG exhibits a specific saturation magnetization (M_s) of 32.8 emu g^{-1} , and the nanocomposites are quickly isolated using a magnetic field following the adsorption process. These results highlight the considerable promise of CFG in the treatment of real industrially used wastewater [116] (Scheme 57).

**Scheme 57.** Removal of methyl orange.

In summary, the efficiency of a variety of carbon-based nanoparticles and their composites towards the removal of various organic pollutants has been represented in Table 1.

Table 1. Efficiency of carbon-based nanoparticles/composites.

Type	Nanoparticles/Composites	Type of Organic Pollutants	Time	Absorption/ Elimination Efficiency of Nanomaterial	Ref.
Magnetic fullerene nanocomposites	Functionalized Magnetic Fullerene Nanocomposites	Methylene Blue Acid Blue 25	45 min 45 min	99.6% 97.01%	[88]
	Functionalized Magnetic Fullerene Nanocomposites	Ciprofloxacin	153 min	65 mg/L	[89]
Magnetic Carbon-dot Nanocomposites	Carbon-dot and magnetite-modified magnetic carbon nanotubes	Carbamazepine	3 h	65 mg/g	[90]
	Magnetic C-Dots	Methylene Blue	30 min	83%	[91]
Magnetic Carbon nanotube nanocomposites	Carbon nanotubes-incorporated MIL-88B-Fe	Phenol	30 min	55%	[93]
	Magnetic CNTs functionalized with polyethylenimine	Alizarin Red S	40 min	94.6%	[95]
	Multiwalled carbon nanotubes	Rose Bengal	30 min	100%	[94]
	Magnetic Carbon-nanotube–Cyclodextrin composite	Methylene Blue	25 h	196.5 mg/g	[95]
	Magnetic graphitized MWCNTs modified with Chitosan	Crystal Violet	100 min	94.56–100%	[96]
	Magnetic polymers multiwall carbon nanotube nanocomposite	Orange (II) Sunset yellow FCF Amaranth	6 h 6 h 6 h	67.57 mg/g 85.47 mg/g 47.39 mg/g	[97]
Magnetic Graphite Nanocomposites	Magnetic-modified multiwalled carbon nanotubes	Methylene Blue Thioflavin Janus Green Crystal Violet	15 min 15 min 15 min 15 min	95% 95% 95% 100%	[98]
	Magnetic carbon nanotubes modified with guar gum GG-MWCNT- Fe_3O_4	Methylene Blue Neutral Red	120 min 20 min	37.4 mg/L 28.9 mg/L	[99]
	Magnetic multiwalled carbon nanotubes	Methylene Blue Neutral Red	60 min 60 min	42.3 mg/g 77.5 mg/g	[100]
	Magnetic graphite intercalation compounds as persulfate activators	Bisphenol A	75 min	99.3%	[101]
	Acid-resistant Magnetic Co/C nanocomposite	Rhodamine B Malachite Green	30 min 30 min	>99% >99%	[102]
	Magnetic Fe_2O_4 –graphite composite	Levofloxacin	15 min	80%	[103]
Magnetic Graphene Nanocomposites	Fe_2O_4 /porous graphene nanocomposite	Methyl Violet	5 min	460 mg/g	[104]
	Magnetic sponge of graphene (Fe_3O_4 -GS)	Methyl blue	5 h	526 mg/g	[105]
	Magnetic photocatalyst of graphene with Fe_3O_4 and NiO GNs/ Fe_3O_4 /NiO nanocomposite	p-Nitrophenol Rhodamine B	20 min	94.1% 86.7%	[106]
	Reduced graphene Oxide (GO) on Fe oxide (GO/ $\text{FeO}.\text{Fe}_2\text{O}_3$)	1-Naphthylamine 1-Naphthol Naphthalene		1.45 mmol/g 1.13 mmol/g 1.05 mmol/g	[107]
	Magnetic composite Fe_3O_4 @graphene	Methylene Blue Congo Red	30 min 30 min	45.27 mg/g 33.66 mg/g	[108]
	Nanocomposites of magnetic CoFe_2O_4 functionalized graphene sheets (CoFe_2O_4 -FGS)	Methyl Orange	60 min	71.54 mg/g	[109]
Magnetic graphene oxide nanocomposites	Graphene-based magnetic nanocomposite (G/ Fe_3O_4)	Fuchsine	30 min	89.4 mg/g	[110]
	Magnetic RCNT-CD	4-Nitrophenol Methylene Blue	10 min 10 min	84% 96%	[111]
	Magnetic CoFe_2O_4 /GO	Methylene Blue Rhodamine B Methyl Orange	7 h 7 h 7 h	355.9 mg/g 284.9 mg/g 53.0 mg/g	[112]
	Mn-doped Fe_3O_4 hollow microspheres on rGO	Rhodamine B	80 min	96.4%	[113]
	GO sheets with Fe_3O_4 nanoparticles	Rhodamine 6G	5 min	89%	[114]
	Reduced graphene oxide (RGO)-supported ferrite (MFe_2O_4 , M = Mn, Zn, Co, Ni)	Methylene Blue Rhodamine B	2 min 2 min	100% 92%	[115]
	Nanocomposite containing CoFe_2O_4 and reduced graphene oxide	Methyl Orange	2 h	263 mg/g	[116]

3. Conclusions and Perspectives

A comprehensive examination of carbon nano-adsorbents, including graphene, graphene oxide, fullerene, carbon dots, graphite and carbon nanotubes has demonstrated their remarkable ability to eliminate organic pollutants, making them an excellent choice for

environmental clean-up. The effectiveness of removing organic pollutants using these materials is attributed to their recyclable nature, low cytotoxicity, homogeneous nanoparticle deposition, and environmentally friendly procedures. While these materials have found extensive use in practical applications for eliminating organic contaminants from wastewater, the cost of carbon nanocomposites and the uncertainty regarding the potential hazards of nanosized carbon compounds persist in environmental systems. Despite the significant impact that these materials can have, there is a need for the development of more green synthesis methods and economical techniques for characterizing them. In the current scenario, the scientific community should shift its focus towards the creation of effective methods utilizing biological agents such as microbes and enzymes. These agents have the potential to break down a variety of organic pollutants and could offer more sustainable solutions.

Author Contributions: B.A.: conceptualization, writing—original draft; writing—reviewing and editing; R.R.: supervision; V.: writing—original draft; M.A.: writing—reviewing and editing; S.A.C.C.: supervision; writing—reviewing and editing. All authors have read and agreed to the published version of the manuscript.

Funding: SACC also acknowledges (FCT/MCTES, Fundação para a Ciência e Tecnologia and Ministério da Ciência, Tecnologia e Ensino Superior) for projects UIDB/50006/2020 and UIDP/50006/2020FCT and for the Scientific Employment Stimulus—Institutional Call (<https://doi.org/10.54499/CEECINST/00102/2018/CP1567/CT0026>).

Institutional Review Board Statement: Not applicable.

Informed Consent Statement: Not applicable.

Data Availability Statement: The data used in this paper are the articles from other authors that were consulted and are available online.

Acknowledgments: The authors would like to express their sincere thanks to the management of Presidency University, Rajanukunte, Itgalpura, Bangalore, India, Baba Mastnath University, Rohtak, Haryana, India, Universidade NOVA de Lisboa, and Islamic Azad University, Shoushtar, Iran for providing the required facilities to write and submit the article for publication. SACC also acknowledges (FCT/MCTES, Fundação para a Ciência e Tecnologia and Ministério da Ciência, Tecnologia e Ensino Superior) for projects UIDB/50006/2020 and UIDP/50006/2020FCT and for the Scientific Employment Stimulus—Institutional Call (DOI 10.54499/CEECINST/00102/2018/CP1567/CT0026).

Conflicts of Interest: The authors declare no conflicts of interest.

References

1. Narain-Ford, D.M.; Bartholomeus, R.P.; Dekker, S.C.; van Wezel, A.P. Natural Purification Through Soils: Risks and Opportunities of Sewage Effluent Reuse in Sub-surface Irrigation. In *Reviews of Environmental Contamination and Toxicology*; Springer: Berlin/Heidelberg, Germany, 2020; Volume 250, pp. 85–117.
2. Pham-Duc, P.; Nguyen-Viet, H.; Hattendorf, J.; Cam, P.D.; Zurbrügg, C.; Zinsstag, J.; Odermatt, P. Diarrhoeal diseases among adult population in an agricultural community Hanam province, Vietnam, with high wastewater and excreta re-use. *BMC Public Health* **2014**, *14*, 1–14. [[CrossRef](#)]
3. Yang, J.; Jia, R.S.; Gao, Y.L.; Wang, W.F.; Cao, P.Q. The reliability evaluation of reclaimed water reused in power plant project. *IOP Conf. Ser. Earth Environ. Sci.* **2017**, *100*, 012189. [[CrossRef](#)]
4. Clemmens, A.J.; Allen, R.G.; Burt, C.M. Technical concepts related to conservation of irrigation and rainwater in agricultural systems. *Water Resour. Res.* **2008**, *44*, W00E03. [[CrossRef](#)]
5. Sato, T.; Qadir, M.; Yamamoto, S.; Endo, T.; Zahoor, A. Global, regional, and country level need for data on wastewater generation, treatment, and use. *Agric. Water Manag.* **2013**, *130*, 1–13. [[CrossRef](#)]
6. Dickin, S.K.; Schuster-Wallace, C.J.; Qadir, M.; Pizzacalla, K. A review of health risks and pathways for exposure to wastewater Use in Agriculture. *Environ. Health Perspect.* **2016**, *124*, 900–909. [[CrossRef](#)]
7. Duan, B.; Zhang, W.; Zheng, H.; Wu, C.; Zhang, Q.; Bu, Y. Comparison of health risk assessments of heavy metals and as in sewage sludge from wastewater treatment plants (WWTPs) for adults and children in the urban district of Taiyuan, China. *Int. J. Environ. Res. Public Health* **2017**, *14*, 1194. [[CrossRef](#)]
8. Carr, R. Who guidelines for safe wastewater use—More than just numbers. *Irrig. Drain.* **2005**, *54* (Suppl. S1), S103–S111. [[CrossRef](#)]

9. Pedrero, F.; Kalavrouziotis, I.; Alarcón, J.J.; Koukoulakis, P.; Asano, T. Use of treated municipal wastewater in irrigated agriculture—Review of some practices in Spain and Greece. *Agric. Water Manag.* **2010**, *97*, 1233–1241. [[CrossRef](#)]
10. Katsoyiannis, I.A.; Gkotsis, P.; Castellana, M.; Cartechini, F.; Zouboulis, A.I. Production of demineralized water for use in thermal power stations by advanced treatment of secondary wastewater effluent. *J. Environ. Manag.* **2017**, *190*, 132–139. [[CrossRef](#)]
11. Chaoua, S.; Boussaa, S.; El Gharmali, A.; Boumezzough, A. Impact of irrigation with wastewater on accumulation of heavy metals in soil and crops in the region of Marrakech in Morocco. *J. Saudi Soc. Agric. Sci.* **2019**, *18*, 429–436. [[CrossRef](#)]
12. Poustie, A.; Yang, Y.; Verburg, P.; Pagilla, K.; Hanigan, D. Reclaimed wastewater as a viable water source for agricultural irrigation: A review of food crop growth inhibition and promotion in the context of environmental change. *Sci. Total Environ.* **2020**, *739*, 139756. [[CrossRef](#)] [[PubMed](#)]
13. Balkhair, K.S. Microbial contamination of vegetable crop and soil profile in arid regions under controlled application of domestic wastewater. *Saudi J. Biol. Sci.* **2016**, *23*, S83–S92. [[CrossRef](#)]
14. Contreras, J.D.; Meza, R.; Siebe, C.; Rodríguez-Dozal, S.; López-Vidal, Y.A.; Castillo-Rojas, G.; Amieva, R.I.; Solano-Gálvez, S.G.; Mazari-Hiriart, M.; Silva-Magaña, M.A.; et al. Health risks from exposure to untreated wastewater used for irrigation in the Mezquital Valley, Mexico: A 25-year update. *Water Res.* **2017**, *123*, 834–850. [[CrossRef](#)] [[PubMed](#)]
15. Singh, A.; Sawant, M.; Kamble, S.J.; Herlekar, M.; Starkl, M.; Aymerich, E.; Kazmi, A. Performance evaluation of a decentralized wastewater treatment system in India. *Environ. Sci. Pollut. Res.* **2019**, *26*, 21172–21188. [[CrossRef](#)]
16. Ungureanu, N.; Vladut, V.; Dincă, M.; Zăbavă, B.-Ş.; Vlăduț, V. Reuse of wastewater for irrigation. A sustainable practice in arid and semi-arid regions. In Proceedings of the 7th International Conference on Thermal Equipment, Renewable Energy and Rural Development (TE-RE-RD), Drobeta-Turnu Severin, Romania, 31 May–2 June 2018.
17. Angelakis, A.N.; Snyder, S.A. Wastewater treatment and reuse: Past, present, and future. *Water* **2015**, *7*, 4887–4895. [[CrossRef](#)]
18. Jeong, H.; Kim, H.; Jang, T. Irrigation water quality standards for indirect wastewater reuse in agriculture: A contribution toward sustainable wastewater reuse in South Korea. *Water* **2016**, *8*, 169. [[CrossRef](#)]
19. Kimura, K.; Honoki, D.; Sato, T. Effective physical cleaning and adequate membrane flux for direct membrane filtration (DMF) of municipal wastewater: Up-concentration of organic matter for efficient energy recovery. *Sep. Purif. Technol.* **2017**, *181*, 37–43. [[CrossRef](#)]
20. Ding, W.; Cheng, S.; Yu, L.; Huang, H. Effective swine wastewater treatment by combining microbial fuel cells with flocculation. *Chemosphere* **2017**, *182*, 567–573. [[CrossRef](#)]
21. Rott, E.; Minke, R.; Steinmetz, H. Removal of phosphorus from phosphonate-loaded industrial wastewaters via precipitation/flocculation. *J. Water Process Eng.* **2017**, *17*, 188–196. [[CrossRef](#)]
22. Lin, C.Y.; Chiang, C.C.; Thi Nguyen, M.L.; Lay, C.H. Enhancement of fermentative biohydrogen production from textile desizing wastewater via coagulation-pretreatment. *Int. J. Hydrogen Energy* **2017**, *42*, 12153–12158. [[CrossRef](#)]
23. Cristóvão, R.O.; Gonçalves, C.; Botelho, C.M.; Martins, R.J.E.; Boaventura, R.A.R. Chemical oxidation of fish canning wastewater by Fenton's reagent. *J. Environ. Chem. Eng.* **2014**, *2*, 2372–2376. [[CrossRef](#)]
24. Li, R.; Yang, C.; Chen, H.; Zeng, G.; Yu, G.; Guo, J. Removal of triazophos pesticide from wastewater with Fenton reagent. *J. Hazard. Mater.* **2009**, *167*, 1028–1032. [[CrossRef](#)] [[PubMed](#)]
25. Defaei, M.; Taheri-Kafrani, A.; Miroliaei, M.; Yaghmaei, P. Improvement of stability and reusability of α -amylase immobilized on naringin functionalized magnetic nanoparticles: A robust nanobiocatalyst. *Int. J. Biol. Macromol.* **2018**, *113*, 354–360. [[CrossRef](#)]
26. Berberidou, C.; Kitsiou, V.; Lambropoulou, D.A.; Antoniadis, A.; Ntonou, E.; Zalidis, G.C.; Poulios, I. Evaluation of an alternative method for wastewater treatment containing pesticides using solar photocatalytic oxidation and constructed wetlands. *J. Environ. Manag.* **2017**, *195*, 133–139. [[CrossRef](#)]
27. Patel, H.; Vashi, R.T. Batch Adsorption Treatment of Textile Wastewater. In *Characterization and Treatment of Textile Wastewater*; Elsevier: Amsterdam, The Netherlands, 2015; pp. 111–125. [[CrossRef](#)]
28. Kyzas, G.Z.; Fu, J.; Lazaridis, N.K.; Bikaris, D.N.; Matis, K.A. New approaches on the removal of pharmaceuticals from wastewaters with adsorbent materials. *J. Mol. Liq.* **2015**, *209*, 87–93. [[CrossRef](#)]
29. de Caprariis, B.; De Filippis, P.; Hernandez, A.D.; Petrucci, E.; Petrullo, A.; Scarsella, M.; Turchi, M. Pyrolysis wastewater treatment by adsorption on biochars produced by poplar biomass. *J. Environ. Manag.* **2017**, *197*, 231–238. [[CrossRef](#)] [[PubMed](#)]
30. Suárez-Iglesias, O.; Collado, S.; Oulego, P.; Díaz, M. Graphene-family nanomaterials in wastewater treatment plants. *Chem. Eng. J.* **2017**, *313*, 121–135. [[CrossRef](#)]
31. Delkash, M.; Ebrazi Bakhshayesh, B.; Kazemian, H. Using zeolitic adsorbents to cleanup special wastewater streams: A review. *Microporous Mesoporous Mater.* **2015**, *214*, 224–241. [[CrossRef](#)]
32. Wang, S.; Peng, Y. Natural zeolites as effective adsorbents in water and wastewater treatment. *Chem. Eng. J.* **2010**, *156*, 11–24. [[CrossRef](#)]
33. Umezuru, E.C.; Mashifana, T.; Kandjou, V.; Amani-Beni, M.; Sadeghifar, H.; Fayazi, M.; Karimi-Maleh, H.; Sithole, N.T. Application of zeolite based nanocomposites for wastewater remediation: Evaluating newer and environmentally benign approaches. *Environ. Res.* **2023**, *231*, 116073. [[CrossRef](#)]
34. Bialczyk, J.; Natkański, P.; Kuśtrowski, P.; Czaja-Prokop, U.; Bober, B.; Kaminski, A. Removal of cyanobacterial anatoxin-a from water by natural clay adsorbents. *Appl. Clay Sci.* **2017**, *148*, 17–24. [[CrossRef](#)]
35. Khan, T.A.; Dahiya, S.; Ali, I. Use of kaolinite as adsorbent: Equilibrium, dynamics and thermodynamic studies on the adsorption of Rhodamine B from aqueous solution. *Appl. Clay Sci.* **2012**, *69*, 58–66. [[CrossRef](#)]

36. Magriots, Z.M.; Leal, P.V.B.; de Sales, P.F.; Papini, R.M.; Viana, P.R.M.; Arroyo, P.A. A comparative study for the removal of mining wastewater by kaolinite, activated carbon and beta zeolite. *Appl. Clay Sci.* **2014**, *91–92*, 55–62. [[CrossRef](#)]
37. Struijk, M.; Rocha, F.; Detellier, C. Novel thio-kaolinite nanohybrid materials and their application as heavy metal adsorbents in wastewater. *Appl. Clay Sci.* **2017**, *150*, 192–201. [[CrossRef](#)]
38. Gil, A.; Assis, F.C.C.; Albeniz, S.; Korili, S.A. Removal of dyes from wastewaters by adsorption on pillared clays. *Chem. Eng. J.* **2011**, *168*, 1032–1040. [[CrossRef](#)]
39. Georgescu, A.M.; Nardou, F.; Zichil, V.; Nistor, I.D. Adsorption of lead(II) ions from aqueous solutions onto Cr-pillared clays. *Appl. Clay Sci.* **2018**, *152*, 44–50. [[CrossRef](#)]
40. Rodrigues Mota, T.L.; Marques de Oliveira, A.P.; Nunes, E.H.M.; Houmar, M. Simple process for preparing mesoporous sol-gel silica adsorbents with high water adsorption capacities. *Microporous Mesoporous Mater.* **2017**, *253*, 177–182. [[CrossRef](#)]
41. Banaei, A.; Samadi, S.; Karimi, S.; Vojoudi, H.; Pourbasheer, E.; Badiei, A. Synthesis of silica gel modified with 2,2'-(hexane-1,6-diylibis(oxy)) dibenzaldehyde as a new adsorbent for the removal of Reactive Yellow 84 and Reactive Blue 19 dyes from aqueous solutions: Equilibrium and thermodynamic studies. *Powder Technol.* **2017**, *319*, 60–70. [[CrossRef](#)]
42. Asfaram, A.; Ghaedi, M.; Ahmadi Azqhandi, M.H.; Goudarzi, A.; Hajati, S. Ultrasound-assisted binary adsorption of dyes onto Mn@CuS/ZnS-NC-AC as a novel adsorbent: Application of chemometrics for optimization and modeling. *J. Ind. Eng. Chem.* **2017**, *54*, 377–388. [[CrossRef](#)]
43. Mazaheri, H.; Ghaedi, M.; Asfaram, A.; Hajati, S. Performance of CuS nanoparticle loaded on activated carbon in the adsorption of methylene blue and bromophenol blue dyes in binary aqueous solutions: Using ultrasound power and optimization by central composite design. *J. Mol. Liq.* **2016**, *219*, 667–676. [[CrossRef](#)]
44. Choleva, T.G.; Gatselou, V.A.; Tsogas, G.Z.; Giokas, D.L. Intrinsic peroxidase-like activity of rhodium nanoparticles, and their application to the colorimetric determination of hydrogen peroxide and glucose. *Microchim. Acta* **2018**, *185*, 22. [[CrossRef](#)]
45. Novais, R.M.; Ascensão, G.; Tobaldi, D.M.; Seabra, M.P.; Labrincha, J.A. Biomass fly ash geopolymers monoliths for effective methylene blue removal from wastewaters. *J. Clean. Prod.* **2018**, *171*, 783–794. [[CrossRef](#)]
46. Habibzadeh, M.; Chaibakhsh, N.; Naeemi, A.S. Optimized treatment of wastewater containing cytotoxic drugs by living and dead biomass of the freshwater microalga, *Chlorella vulgaris*. *Ecol. Eng.* **2018**, *111*, 85–93. [[CrossRef](#)]
47. Vukelic, D.; Boskovic, N.; Agarski, B.; Radonic, J.; Budak, I.; Pap, S.; Sekulic, M.T. Eco-design of a low-cost adsorbent produced from waste cherry kernels. *J. Clean. Prod.* **2018**, *174*, 1620–1628. [[CrossRef](#)]
48. Anjum, M.; Miandad, R.; Waqas, M.; Gehany, F.; Barakat, M.A. Remediation of wastewater using various nano-materials. *Arab. J. Chem.* **2019**, *12*, 4897–4919. [[CrossRef](#)]
49. Tripathi, A.; Rawat Ranjan, M. Heavy Metal Removal from Wastewater Using Low Cost Adsorbents. *J. Bioremediat. Biodegrad.* **2015**, *6*, 315. [[CrossRef](#)]
50. Abbaszadeh, S.; Wan Alwi, S.R.; Webb, C.; Ghasemi, N.; Muhamad, I.I. Treatment of lead-contaminated water using activated carbon adsorbent from locally available papaya peel biowaste. *J. Clean. Prod.* **2016**, *118*, 210–222. [[CrossRef](#)]
51. Reck, I.M.; Paixão, R.M.; Bergamasco, R.; Vieira, M.F.; Vieira, A.M.S. Removal of tartrazine from aqueous solutions using adsorbents based on activated carbon and *Moringa oleifera* seeds. *J. Clean. Prod.* **2018**, *171*, 85–97. [[CrossRef](#)]
52. Lladó, J.; Gil, R.R.; Lao-Luque, C.; Solé-Sardans, M.; Fuente, E.; Ruiz, B. Highly microporous activated carbons derived from biocollagenic wastes of the leather industry as adsorbents of aromatic organic pollutants in water. *J. Environ. Chem. Eng.* **2017**, *5*, 2090–2100. [[CrossRef](#)]
53. Bendi, A.; Dharma Rao, G.B.; Sharma, N.; Singh, M.P. Results in Chemistry CoFe₂O₄/Cu(OH)₂ Nanocomposite: Expeditious and magnetically recoverable heterogeneous catalyst for the four component Biginelli/transesterification reaction and their DFT studies. *Results Chem.* **2021**, *3*, 100202. [[CrossRef](#)]
54. Bendi, A.; Dharma Rao, G.B.; Nancy; Nagakalyan, S. Synthesis and DFT studies of 1,2-disubstituted benzimidazoles using expeditious and magnetically recoverable CoFe₂O₄/Cu(OH)₂ nanocomposite under solvent-free condition. *J. Saudi Chem. Soc.* **2021**, *25*, 101394. [[CrossRef](#)]
55. Farghali, A.A.; Bahgat, M.; Enaiet Allah, A.; Khedr, M.H. Adsorption of Pb(II) ions from aqueous solutions using copper oxide nanostructures. *Beni-Suef Univ. J. Basic Appl. Sci.* **2013**, *2*, 61–71. [[CrossRef](#)]
56. Dissanayake, M.A.K.L.; Divarathna, H.K.D.W.M.N.; Dissanayake, C.B.; Senadeera, G.K.R.; Ekanayake, P.M.P.C.; Thotawattage, C.A. An innovative TiO₂ nanoparticle/nanofibre/nanoparticle, three layer composite photoanode for efficiency enhancement in dye-sensitized solar cells. *J. Photochem. Photobiol. A Chem.* **2016**, *322–323*, 110–118. [[CrossRef](#)]
57. Muhamad, S.U.; Idris, N.H.; Yusoff, H.M.; Din, M.F.M.; Majid, S.R. In-situ encapsulation of nickel nanoparticles in polypyrrole nanofibres with enhanced performance for supercapacitor. *Electrochim. Acta* **2017**, *249*, 9–15. [[CrossRef](#)]
58. Carabineiro, S.A.C.; Dharma Rao, G.B.; Singh, L.; Anjaneyulu, B.; Afshari, M. CuFe₂O₄ Magnetic Nanoparticles as Heterogeneous Catalysts for Synthesis of Dihydropyrimidinones as Inhibitors of SARS-CoV-2 Surface Proteins—Insights from Molecular Docking Studies. *Processes* **2023**, *11*, 2294. [[CrossRef](#)]
59. Asfaram, A.; Ghaedi, M.; Goudarzi, A.; Rajabi, M. Response surface methodology approach for optimization of simultaneous dye and metal ion ultrasound-assisted adsorption onto Mn doped Fe₃O₄-NPs loaded on AC: Kinetic and isothermal studies. *Dalton Trans.* **2015**, *44*, 14707–14723. [[CrossRef](#)]
60. Ganesan, V.; Louis, C.; Damodaran, S.P. Graphene oxide-wrapped magnetite nanoclusters: A recyclable functional hybrid for fast and highly efficient removal of organic dyes from wastewater. *J. Environ. Chem. Eng.* **2018**, *6*, 2176–2190. [[CrossRef](#)]

61. Asfaram, A.; Ghaedi, M.; Hajati, S.; Goudarzi, A. Ternary dye adsorption onto MnO₂ nanoparticle-loaded activated carbon: Derivative spectrophotometry and modeling. *RSC Adv.* **2015**, *5*, 72300–72320. [\[CrossRef\]](#)
62. Anjaneyulu, B.; Chirnmay; Chauhan, V.; Sonia, A.C.C.; Mozhgan, A. Recent advances on zinc ferrite and its derivatives as the forerunner of the nanomaterials in catalytic applications. *J. Inorg. Organomet. Polym.* **2023**, *1*–21. [\[CrossRef\]](#)
63. Siqueira, J.R.; Oliveira, O.N. 9–Carbon-Based Nanomaterials. In *Nanostructures*; Elsevier: Oxford, UK, 2017. [\[CrossRef\]](#)
64. Ren, X.; Zeng, G.; Tang, L.; Wang, J.; Wan, J.; Feng, H.; Song, B.; Huang, C.; Tang, X. Effect of exogenous carbonaceous materials on the bioavailability of organic pollutants and their ecological risks. *Soil Biol. Biochem.* **2018**, *116*, 70–81. [\[CrossRef\]](#)
65. Yang, Y.; Yang, X.; Yang, Y.; Yuan, Q. Aptamer-functionalized carbon nanomaterials electrochemical sensors for detecting cancer relevant biomolecules. *Carbon* **2018**, *129*, 380–395. [\[CrossRef\]](#)
66. Malhotra, B.D.; Ali, M.A. Functionalized Carbon Nanomaterials for Biosensors. In *Nanomaterials for Biosensors*; Elsevier: Amsterdam, The Netherlands, 2018; Chapter 2; pp. 75–103. [\[CrossRef\]](#)
67. Kwon, Y.J.; Kim, Y.; Jeon, H.; Cho, S.; Lee, W.; Lee, J.U. Graphene/carbon nanotube hybrid as a multi-functional interfacial reinforcement for carbon fiber-reinforced composites. *Compos. Part B Eng.* **2017**, *122*, 23–30. [\[CrossRef\]](#)
68. Imani Yengejeh, S.; Kazemi, S.A.; Öchsner, A. Carbon nanotubes as reinforcement in composites: A review of the analytical, numerical and experimental approaches. *Comput. Mater. Sci.* **2017**, *136*, 85–101. [\[CrossRef\]](#)
69. Chen, Y.F.; Tan, Y.J.; Li, J.; Hao, Y.B.; Shi, Y.D.; Wang, M. Graphene oxide-assisted dispersion of multi-walled carbon nanotubes in biodegradable Poly(ϵ -caprolactone) for mechanical and electrically conductive enhancement. *Polym. Test.* **2018**, *65*, 387–397. [\[CrossRef\]](#)
70. Deb, A.; Vimala, R. Camptothecin loaded graphene oxide nanoparticle functionalized with polyethylene glycol and folic acid for anticancer drug delivery. *J. Drug Deliv. Sci. Technol.* **2018**, *43*, 333–342. [\[CrossRef\]](#)
71. Ahmed, W.; Elhissi, A.; Dhanak, V.; Subramani, K. Carbon nanotubes: Applications in cancer therapy and drug delivery research. In *Emerging Nanotechnologies in Dentistry*; Elsevier: Amsterdam, The Netherlands, 2017; pp. 371–389. [\[CrossRef\]](#)
72. Ioniță, M.; Crică, L.E.; Voicu, S.I.; Dinescu, S.; Miculescu, F.; Costache, M.; Iovu, H. Synergistic effect of carbon nanotubes and graphene for high performance cellulose acetate membranes in biomedical applications. *Carbohydr. Polym.* **2018**, *183*, 50–61. [\[CrossRef\]](#)
73. Li, Z.-F.; Xin, L.; Yang, F.; Liu, Y.; Liu, Y.; Zhang, H.; Stanciu, L.; Xie, J. Hierarchical polybenzimidazole-grafted graphene hybrids as supports for Pt nanoparticle catalysts with excellent PEMFC performance. *Nano Energy* **2015**, *16*, 281–292. [\[CrossRef\]](#)
74. Jeng, K.T.; Hsu, N.Y.; Chien, C.C. Synthesis and evaluation of carbon nanotube-supported RuSe catalyst for direct methanol fuel cell cathode. *Int. J. Hydrogen Energy* **2011**, *36*, 3997–4006. [\[CrossRef\]](#)
75. Teow, Y.H.; Mohammad, A.W. New generation nanomaterials for water desalination: A review. *Desalination* **2019**, *451*, 2–17. [\[CrossRef\]](#)
76. Thines, R.K.; Mubarak, N.M.; Nizamuddin, S.; Sahu, J.N.; Abdullah, E.C.; Ganesan, P. Application potential of carbon nanomaterials in water and wastewater treatment: A review. *J. Taiwan Inst. Chem. Eng.* **2017**, *72*, 116–133. [\[CrossRef\]](#)
77. Ray, S.C.; Jana, N.R. Application of Carbon-Based Nanomaterials for Removal of Biologically Toxic Materials. In *Carbon Nanomaterials for Biological and Medical Applications*; Elsevier: Amsterdam, The Netherlands, 2017; pp. 43–86. [\[CrossRef\]](#)
78. Kong, L.P.; Gan, X.J.; bin Ahmad, A.L.; Hamed, B.H.; Evarts, E.R.; Ooi, B.S.; Lim, J. Design and synthesis of magnetic nanoparticles augmented microcapsule with catalytic and magnetic bifunctionalities for dye removal. *Chem. Eng. J.* **2012**, *197*, 350–358. [\[CrossRef\]](#)
79. Lotfi Zadeh Zhad, H.R.; Aboufazeli, F.; Sadeghi, O.; Amani, V.; Najafi, E.; Tavassoli, N. Tris(2-Aminoethyl)amine-functionalized Femagnetic nanoparticles as a selective sorbent for separation of silver and gold ions in different pHs. *J. Chem.* **2013**, *2013*, 482793. [\[CrossRef\]](#)
80. Carreño, N.L.V.; Escote, M.T.; Valentini, A.; McCafferty, L.; Stolojan, V.; Beliatis, M.; Mills, C.A.; Rhodes, R.; Smith, C.T.G.; Silva, S.R.P. Adsorbent 2D and 3D carbon matrices with protected magnetic iron nanoparticles. *Nanoscale* **2015**, *7*, 17441–17449. [\[CrossRef\]](#)
81. Chen, C.L.; Wang, X.K.; Nagatsu, M. Europium adsorption on multiwall carbon nanotube/iron oxide magnetic composite in the presence of polyacrylic acid. *Environ. Sci. Technol.* **2009**, *43*, 2362–2367. [\[CrossRef\]](#)
82. Lu, A.H.; Salabas, E.L.; Schüth, F. Magnetic nanoparticles: Synthesis, protection, functionalization, and application. *Angew. Chem. Int. Ed.* **2007**, *46*, 1222–1244. [\[CrossRef\]](#)
83. Yu, C.; Geng, J.; Zhuang, Y.; Zhao, J.; Chu, L.; Luo, X. Preparation of the chitosan grafted poly (quaternary ammonium)/Fe₃O₄ nanoparticles and its adsorption performance for food yellow 3. *Carbohydr. Polym.* **2016**, *152*, 327–336. [\[CrossRef\]](#)
84. Sayana, K.V.; Prajwal, K.; Deeksha, K.J.; Vishalakshi, B.; Vishwanath, T. Magnetized CNTs incorporated MBA cross-linked guar gum nano-composite for methylene blue dye removal. *J. Appl. Polym. Sci.* **2024**, *141*, e54868. [\[CrossRef\]](#)
85. Ege, K.; Arzum, Ç.; Alattin, Ç.; Elif, A. Enhanced photocatalytic dye degradation using surface-modified tungstophosphoric acid-iron magnetic nanocatalyst. *Opt. Mater.* **2024**, *148*, 114816. [\[CrossRef\]](#)
86. Zhao, C.; Wang, X.; Zhang, S.; Sun, N.; Zhou, H.; Wang, G.; Zhang, Y.; Zhang, H.; Zhao, H. Porous carbon nanosheets functionalized with Fe₃O₄ nanoparticles for capacitive removal of heavy metal ions from water. *Environ. Sci. Water Res. Technol.* **2020**, *6*, 331–340. [\[CrossRef\]](#)
87. Yang, W.; Chen, H.; Han, X.; Ding, S.; Shan, Y.; Liu, Y. Preparation of magnetic Co-Fe modified porous carbon from agricultural wastes by microwave and steam activation for mercury removal. *J. Hazard. Mater.* **2020**, *5*, 120981. [\[CrossRef\]](#) [\[PubMed\]](#)

88. Elessawy, N.A.; El-Sayed, E.M.; Ali, S.; Elkady, M.F.; Elnouby, M.; Hamad, H.A. One-pot green synthesis of magnetic fullerene nanocomposite for adsorption characteristics. *J. Water Process Eng.* **2020**, *34*, 101047. [\[CrossRef\]](#)
89. Elessawy, N.A.; Elnouby, M.; Gouda, M.H.; Hamad, H.A.; Taha, N.A.; Gouda, M.; Eldin, M.S.M. Ciprofloxacin removal using magnetic fullerene nanocomposite obtained from sustainable PET bottle wastes: Adsorption process optimization, kinetics, isotherm, regeneration and recycling studies. *Chemosphere* **2020**, *239*, 124728. [\[CrossRef\]](#)
90. Deng, Y.; Ok, Y.S.; Mohan, D.; Pittman, C.U.; Dou, X. Carbamazepine removal from water by carbon dot-modified magnetic carbon nanotubes. *Environ. Res.* **2019**, *169*, 434–444. [\[CrossRef\]](#)
91. Sun, A.C. Synthesis of magnetic carbon nanodots for recyclable photocatalytic degradation of organic compounds in visible light. *Adv. Powder Technol.* **2018**, *29*, 719–725. [\[CrossRef\]](#)
92. Zhang, H.; Chen, S.; Zhang, H.; Fan, X.; Gao, C.; Yu, H.; Quan, X. Carbon nanotubes-incorporated MIL-88B-Fe as highly efficient Fenton-like catalyst for degradation of organic pollutants. *Front. Environ. Sci. Eng.* **2019**, *13*, 18. [\[CrossRef\]](#)
93. Zhang, Z.; Chen, H.; Wu, W.; Pang, W.; Yan, G. Efficient removal of Alizarin Red S from aqueous solution by polyethyleneimine functionalized magnetic carbon nanotubes. *Bioresour. Technol.* **2019**, *293*, 122100. [\[CrossRef\]](#)
94. Salam, M.A.; El-Shishtawy, R.M.; Obaid, A.Y. Synthesis of magnetic multi-walled carbon nanotubes/magnetite/chitin magnetic nanocomposite for the removal of Rose Bengal from real and model solution. *J. Ind. Eng. Chem.* **2014**, *20*, 3559–3567. [\[CrossRef\]](#)
95. Cheng, J.; Chang, P.R.; Zheng, P.; Ma, X. Characterization of magnetic carbon nanotube-cyclodextrin composite and its adsorption of dye. *Ind. Eng. Chem. Res.* **2014**, *53*, 1415–1421. [\[CrossRef\]](#)
96. Zhu, H.; Fu, Y.; Jiang, R.; Yao, J.; Liu, L.; Chen, Y.; Xiao, L.; Zeng, G. Preparation, characterization and adsorption properties of chitosan modified magnetic graphitized multi-walled carbon nanotubes for highly effective removal of a carcinogenic dye from aqueous solution. *Appl. Surf. Sci.* **2013**, *285*, 865–873. [\[CrossRef\]](#)
97. Gao, H.; Zhao, S.; Cheng, X.; Wang, X.; Zheng, L. Removal of anionic azo dyes from aqueous solution using magnetic polymer multi-wall carbon nanotube nanocomposite as adsorbent. *Chem. Eng. J.* **2013**, *223*, 84–90. [\[CrossRef\]](#)
98. Madrakian, T.; Afkhami, A.; Ahmadi, M.; Bagheri, H. Removal of some cationic dyes from aqueous solutions using magnetic-modified multi-walled carbon nanotubes. *J. Hazard. Mater.* **2011**, *196*, 109–114. [\[CrossRef\]](#)
99. Yan, L.; Chang, P.R.; Zheng, P.; Ma, X. Characterization of magnetic guar gum-grafted carbon nanotubes and the adsorption of the dyes. *Carbohydr. Polym.* **2012**, *87*, 1919–1924. [\[CrossRef\]](#)
100. Qu, S.; Huang, F.; Yu, S.; Chen, G.; Kong, J. Magnetic removal of dyes from aqueous solution using multi-walled carbon nanotubes filled with Fe₂O₃ particles. *J. Hazard. Mater.* **2008**, *160*, 643–647. [\[CrossRef\]](#)
101. Ranjbar, E.; Ghiassi, R.; Baghdadi, M.; Ruhl, A.S. Bisphenol A removal in treated wastewater matrix at neutral pH using magnetic graphite intercalation compounds as persulfate activators. *Water Environ. Res.* **2023**, *95*, e10835. [\[CrossRef\]](#)
102. Ruan, C.P.; Ai, K.L.; Lu, L.H. An Acid-resistant Magnetic Co/C Nanocomposite for Adsorption and Separation of Organic Contaminants from Water. *Chin. J. Anal. Chem.* **2016**, *44*, 224–231. [\[CrossRef\]](#)
103. Wang, L.; Zhao, Q.; Hou, J.; Yan, J.; Zhang, F.; Zhao, J.; Ding, H.; Li, Y.; Ding, L. One-step solvothermal synthesis of magnetic Fe₃O₄-graphite composite for Fenton-like degradation of levofloxacin. *J. Environ. Sci. Health Part A Toxic/Hazard. Subst. Environ. Eng.* **2016**, *51*, 52–62. [\[CrossRef\]](#)
104. Bharath, G.; Alseainat, E.; Ponpandian, N.; Khan, M.A.; Siddiqui, M.R.; Ahmed, F.; Alsharaeh, E.H. Development of adsorption and electrosorption techniques for removal of organic and inorganic pollutants from wastewater using novel magnetite/porous graphene-based nanocomposites. *Sep. Purif. Technol.* **2017**, *188*, 206–218. [\[CrossRef\]](#)
105. Yu, B.; Zhang, X.; Xie, J.; Wu, R.; Liu, X.; Li, H.; Chen, F.; Yang, H.; Ming, Z.; Yang, S.-T. Magnetic graphene sponge for the removal of methylene blue. *Appl. Surf. Sci.* **2015**, *351*, 765–771. [\[CrossRef\]](#)
106. Zhao, G.; Mo, Z.; Zhang, P.; Wang, B.; Zhu, X.; Guo, R. Synthesis of graphene/Fe₃O₄/NiO magnetic nanocomposites and its application in photocatalytic degradation the organic pollutants in wastewater. *J. Porous Mater.* **2015**, *22*, 1245–1253. [\[CrossRef\]](#)
107. Yang, X.; Li, J.; Wen, T.; Ren, X.; Huang, Y.; Wang, X. Adsorption of naphthalene and its derivatives on magnetic graphene composites and the mechanism investigation. *Colloids Surf. A Physicochem. Eng. Asp.* **2013**, *422*, 118–125. [\[CrossRef\]](#)
108. Yao, Y.; Miao, S.; Liu, S.; Ma, L.P.; Sun, H.; Wang, S. Synthesis, characterization, and adsorption properties of magnetic Fe₃O₄@graphene nanocomposite. *Chem. Eng. J.* **2012**, *184*, 326–332. [\[CrossRef\]](#)
109. Li, N.; Zheng, M.; Chang, X.; Ji, G.; Lu, H.; Xue, L.; Pan, L.; Cao, J. Preparation of magnetic CoFe₂O₄-functionalized graphene sheets via a facile hydrothermal method and their adsorption properties. *J. Solid State Chem.* **2011**, *184*, 953–958. [\[CrossRef\]](#)
110. Wang, C.; Feng, C.; Gao, Y.; Ma, X.; Wu, Q.; Wang, Z. Preparation of a graphene-based magnetic nanocomposite for the removal of an organic dye from aqueous solution. *Chem. Eng. J.* **2011**, *173*, 92–97. [\[CrossRef\]](#)
111. Islam, M.R.; Ferdous, M.; Sujan, M.I.; Mao, X.; Zeng, H.; Azam, M.S. Recyclable Ag-decorated highly carbonaceous magnetic nanocomposites for the removal of organic pollutants. *J. Colloid Interface Sci.* **2020**, *562*, 52–62. [\[CrossRef\]](#)
112. Chang, S.; Zhang, Q.; Lu, Y.; Wu, S.; Wang, W. High-efficiency and selective adsorption of organic pollutants by magnetic CoFe₂O₄/graphene oxide adsorbents: Experimental and molecular dynamics simulation study. *Sep. Purif. Technol.* **2020**, *238*, 119400. [\[CrossRef\]](#)
113. Chen, Z.; Zheng, Y.; Liu, Y.; Zhang, W.; Wang, Y.; Guo, X.; Tang, X.; Zhang, Y.; Wang, Z.; Zhang, T. Magnetic Mn-Doped Fe₃O₄ hollow Microsphere/RGO heterogeneous Photo-Fenton Catalyst for high efficiency degradation of organic pollutant at neutral pH. *Mater. Chem. Phys.* **2019**, *238*, 121893. [\[CrossRef\]](#)

114. Mishra, A. Study of organic pollutant removal capacity for magnetite@ graphene oxide nanocomposites. *Vacuum* **2018**, *157*, 524–529. [[CrossRef](#)]
115. Bai, S.; Shen, X.; Zhong, X.; Liu, Y.; Zhu, G.; Xu, X.; Chen, K. One-pot solvothermal preparation of magnetic reduced graphene oxide-ferrite hybrids for organic dye removal. *Carbon* **2012**, *50*, 2337–2346. [[CrossRef](#)]
116. Song, Z.J.; Ran, W.; Wei, F.Y. One-step approach for the synthesis of CoFe₂O₄ @rGO core-shell nanocomposites as efficient adsorbent for removal of organic pollutants. *Water Sci. Technol.* **2017**, *75*, 397–405. [[CrossRef](#)]

Disclaimer/Publisher’s Note: The statements, opinions and data contained in all publications are solely those of the individual author(s) and contributor(s) and not of MDPI and/or the editor(s). MDPI and/or the editor(s) disclaim responsibility for any injury to people or property resulting from any ideas, methods, instructions or products referred to in the content.